Chapter 3

Title: Synthesis of biocompatible, BSA capped fluorescent $CaCO_3$ pre-nucleation nanoclusters for cell imaging applications.

3.1 Introduction

The reasonable biocompatibility, high quantum yield, small size, and high photostability of fluorescent nanoclusters instigated its applications in the area of bioimaging and nanotherapeutics[315]. Due to these properties, fluorescent nanoclusters can be realized as potential alternatives to popularly used Quantum dots (Qd's). Qd's became popular due to their multicolor size-tunable fluorescence emission with high quantum yield, constant emission output without photobleaching, versatile surface functionalization and highly tunable chemical synthesis[316]. Despite of its large popularity and wide application in various areas, leaching of its constitutent heavy metals in the biological samples[317] and environment[318-321] raised serious concerns. Besides its fewer applications in bioimaging and therapeuitics due to its poor biocompatibility encouraged development of new fluorescent nanoclusters.

Nanoclusters are formed when bulk materials are reduced to the size equivalent to the fermi wavelength[322, 323] (~1-10 nm), imparting unique property to the material-fluorescence. Nanoclusters are popularly synthesized and stabilized by proteins, peptides, polymers, and dendrimers, as a growth template, offering great size control and colloidal stability.[213, 324] Such reduction to sub- nanoscale size unfolds interesting physicochemical, optical and electronic properties, leading to its seamless application in the area of nanomedicine, sensing, catalysis, displays and optical devices.[71, 324-328]

Depending upon the application, various noble metals such as Cu, Ag, and Au have been used for nanocluster synthesis. These materials are known to be environmentally inert and

biocompatible and therefore, perfect for the development of fluorescent nanoclusters for bioimaging applications.[62] Gold nanoclusters are known to be highly biocompatible, leading to its wide application in the area of bioimaging and nanomedicine. However, such biocompatibility is limited for the short term use. It has been demonstrated that, less than 5% gold, present in the BSA protected fluorescent gold nanoclusters, could be metabolized after 28 days. Further it has been shown that on injection of BSA protected fluorescent gold nanoclusters to the mice, infections and damage of vital organs such as liver and kidney occurred, after 28 days of injection.[154]

Despite of noble behaviour of gold (E^0 = +1.498 V) in comparison to other metals in the same group viz. Cu (E^0 = +0.34 V) and Ag (E^0 = +0.7996 V), number of studies have demonstrated that accumulation of BSA protected fluorescent gold nanoclusters in the liver and spleen, results in unrecoverable toxic response.[154, 329-331]On the other hand, alkaline earth metals, such as magnesium (Mg) and calcium (Ca), are physiological elements and play an important role in maintaining the hemostasis.[332] For instance, phosphate clusters, found in the cytoplasm and nucleus, interact with magnesium ions, forming metal phosphate aggregates. These aggregates help in maintaining the positional integrity of phosphate clusters inside cells.[213, 332, 333]Whereas, calcium assists in bone formation, muscular contraction, heartbeat regulation, fluid balance within cells,[334] which controls osmotic pressure, biomineralization, biocatalysis, cell-signaling, metabolism etc.[335-337] Such advantages make calcium as the preferred material of choice for biological applications. However, its high reactivity offers great difficulty in the synthesis and colloidal stability. In this context, number of synthesis routes for Ca and Mg development have been reported. For example, synthesis of 10,12-pentacosadiynoic acid protected amorphous calcium carbonate nanoclusters (1.4 nm) (ACC). These ACC nanoclusters were composed of 7 units of $CaCO_3$.[245] Similarly,

ACC nanoclusters (4.9 nm) were synthesized using 10,12-pentacosadiynoic acid in ethanol and $NaHCO_3$ as a source of CO_2 by a solvothermal approach.[244]

The computerized simulations on $CaCO_3$ mineral nanoclusters indicated that $CaCO_3$ minerals were composed of ionic polymer, with alternating units of calcium (Ca^{2+}) and carbonate (CO_3^{2-}) ions.[338] Yes, indeed, Calcium 2+ is relatively stable. Still, here we are dealing with the stability of two ions together, Ca^{2+} and CO_3^{2-}, which are prone to nucleating due to high surface energy at the nanoscale. Hence, we are trying to stabilize whole calcium carbonate ($CaCO_3$) prenucleation clusters by controlling nucleation and growth processes of Ca^{2+} cations with CO_3^{2-} anions at the nanoscale. Therefore, our dissertation is focused on the stability of ionic clusters Ca^{2+} and CO_3^{2-} together without nucleation, which can lead to uncontrollable growth and aggregation when not stabilized at the nanoscale.

Further studies, based ion-pair and activity approach, demonstrated stabilization of amorphous, pre-nucleation $CaCO_3$ nanoclusters.[339] Studies have shown that on the inclusion of the activator impurities, crystalline (Calcite) $CaCO_3$ can be rendered fluorescent. For instance, room tempertature synthesis of calcite crystals by doping Eu^{3+} and Gd^{3+} rendered these crystals fluorescent. These crystals ($CaCO_3$: 0.02 Gd^{3+}) displayed long fluorescence life-time (6.19 ms) (Exc/ Em = 274/311 nm) due to $^6P_{7/2}$-$^8S_{7/2}$ transition.[247] Whereas, Mn^{2+} doped fluorescent calcite crystal (Ex/Em 325/625nm) displayed a fluorescence lifetime of 50 ms (Temperature=120K)[248], due to 3d→3d transition. The Ce^{3+} and Mn^{2+} doped calcite crystal displayed blue emission (Ex. at 400 nm) due to 5d→4f transition, peculiar to $Ce.^{3+}$ [249] In general, exceptionally high fluorescence lifetimes (~ms) were observed for the dopants Ce^{3+}, Mn^{2+}, Gd^{3+}or Eu^{3+}. Due to their larger sizes, the fore-mentioned crystals were mostly used as phosphors.[340] In addition to these reports, highly biodegradable, fluorescent calcium carbonate and

carbon dot (CD) nanocomposites have also been reported.[251] Furthermore, sulfonated fluorescent dyes were incorporated into the calcite crystal for creating a stable and biocompatible system to understand the mechanism of additive obstruction into the calcite crystal plane, during the dye incorporation. Based on this understanding, a stable, fluorescent, biocompatible white light-emitting system was developed.[336] Briefly, mostly reported $CaCO_3$ prenucleation nanoclusters have not been suggested as a fluorescent, till now. While those Calcite ($CaCO_3$) crystals, which exhibited fluorescence, were synthesized using complex doping processes.

In a completely different approach, BSA protected fluorescent magnesium nanoclusters (Mg-S) were developed from its chloride salt ($MgCl_2$). The developed nanoclusters fluoresced in blue (with 0.17 quantum yield) and green regions. These Mg-S nanoclusters were used for A549 cells bioimaging. It was found that in absence of BSA, high reactivity of Mg led to the poor size control, and colloidal stability which restricted the formation of Mg^0 nanoclusters. The addition of bovine serum albumin (BSA) protein has been suggested to potentially address such issues. However, Mg-S nanoclusters displayed limited colour emission, substantial quantum yield, and low cytotoxicity.[213] It is important to note that above study relied on bio-mineralization process[253, 341] for the formation of Mg-S nanoclusters and certainly very appealing.

Using such technique, ultrafine highly fluorescent red-light emitting gold clusters[90] have been synthesized. Consequently, ultrafine (~1 nm) pre-nucleation fluorescent calcium carbonate nanoclusters can be synthesized, using leaf extract as reducing agent. Although, leaf extract can only facilitate the primary nucleation, capping agents such as BSA may provide the size control at the nanocluster level. Whereas, its tertiary structure consists of 35 cysteine residues with 17 disulfide bonds. These disulfide bonds interact with the nanostructures and protect it from further growth[213, 254, 342]. It will,

therefore, be interesting to synthesize nanocluster using biomineralization process in conjunction with BSA protein. Such green synthesis is an efficient, eco-friendly, non-toxic and low-cost approach in comparison to the chemical as well as microbe mediated synthesis.[343, 344]

The stem peel granulates have been used to synthesize calcium carbonate nanoparticles previously. A stable calcium carbonate nanoparticles (45~75 nm) were synthesized using phenolic reducing agents,[343]extracted from B. ovalifoliolata plant stem peel granulates. Similarly, Moringa oleifera (M. oleifera) flower extract has been used in the synthesis of gold nanoparticles (3-5 nm). M.oleifera leaf extract is known to contain an ample amount of phenolic groups like ascorbic acid[342], which can help in reducing the metal ions[343, 345]during the nanoparticle synthesis. Besides, M.oleifera extract is known to have anti-inflammatory, anti-hypertensive, hepatoprotective and anti-tumor properties.[258, 342] This makes M.oleifera leaf extract, suitable for the synthesis of fluorescent, pre-nucleation calcium carbonate nanoclusters. In addition, obtaining multi-color fluorescence by single fluorescent entity without using any external doping agents has been recognized as a major challenge.[346]

Herein, we, therefore, report, for the first time, facile synthesis of ultrafine (~1 nm) highly biocompatible and photostable, water soluble, inexpensive, BSA capped novel fluorescent $CaCO_3$ pre nucleation nanoclusters (FCPN), for multi-color imaging using MG-63 cell lines. Furthermore, in the current study, we present various spectroscopic and microscopic studies to understand the mechanism behind the fluorescence, and synthesis, besides materials physicochemical characterizations.

3.2 Experimental Section

3.2.1 Synthesis of FCPN

Before performing the experiment, Aqua Regia (HCl:HNO_3=3:1 by volume) was used to wash the glass wares, followed by rinsing through DI water and ethanol. Fresh, M.oleifera leaves (10 g) were collected from the plant and washed thoroughly with Deionized (DI) water. The M.oleifera leaf extract was prepared by pouring leaves (10 g) in a beaker containing DI water (100 ml), followed by heating the beaker at 95 ±2 ^{0}C for 5 hrs on a hot plate. The temprature of the solution was measured using K-type thermocouple. Whatmann No. 1 filter was used to separate Moringa leaf liquid extract (filtrate) from solid residues. The filtrate was used as- prepared. Next, BSA capped fluorescent FCPN and control were prepared.

Briefly, for FCPN, $CaCl_2$ (10 mM) (Avantor Performance Materials) solution in DI water (50 ml) was mixed with of Moringa leaf extract (15 ml) and aqueous ammonical solution (1M) in DI water (2 ml) (SRL Pvt. Ltd., India). The stirred reaction mixture was kept at 55 °C in the conical flask, followed by addition BSA protein solution (5.15 mM) (SRL Pvt. Ltd., India) in DI water (5 ml) and sodium hydroxide (1M) in DI water (1 ml) (SRL Pvt. Ltd., India) for 1 hr (Total solution volume =73 ml). The reaction mixture was incubated at 55 °C for 15 hrs. After 15 hrs of reaction, the solution color gets changed from light yellow to deep yellow and the reaction is terminated.

Control experiment was performed to check the fluorescence spectra by mixing 10 mM $CaCl_2$ (50 ml) and moringa leaf extract (15 ml), 1M NH_4OH (2 ml), 1M NaOH (1 ml) and DI water (5 ml) without capping agent BSA. The entire reaction mixture was incubated at the similar temperature (55 °C) for 15 hrs after stirring for 1 hr duration. The resulting

synthesis procedure for control, produces large size $CaCO_3$ nanoparticles, (~49 nm) (Figure 3.1).

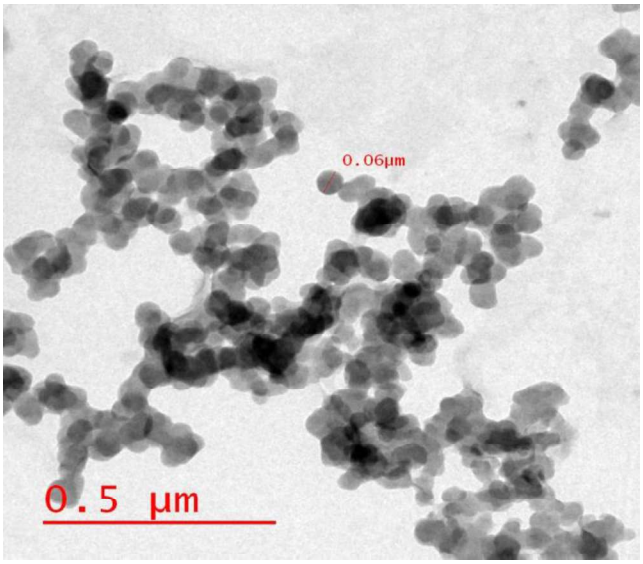

Figure 3.1 TEM image of large size $CaCO_3$ Nanoparticles (NP'S) ~49 nm (Control A) synthesized (without BSA), using leaf extract of Moringa oleifera as reducing agent.

3.2.2 Cell Culture and FCPN Treatment

The cytocompatibility of FCPN was examined using osteoblastic MG-63 cell line (NCCS Pune). MG-63 cells were cultured in Dulbecco's modified Eagle's medium (DMEM) (HIMEDIA), supplemented with 15 % fetal bovine serum (FBS) (GIBCO) and 1 % antibiotics (GIBCO), and incubated in a humidified 5 % CO_2 incubator (Thermo scientific Heracellvios 160i) at 37ºC. At 70-80% confluency, the cells were trypsinized and thereafter, equal amount of cells (10^4 cells/ml) were seeded on glass cover slip in 24 well plates for 24 h. After the stipulated time period, cells were exposed to different concentrations of FCPN (F100, F1000, WF100, and WF1000; diluted in growth media) and incubated further in CO_2 incubator. The cell culture media have been replaced at a regular interval of 48 hrs. Here, F and WF correspond to filtered ones via centrifugation through Amicon Ultra-0.5 ml tubes (F) (Merck and Thermo Fisher Scientific) and non-

filtred supernatant, collected after centrifugation through Eppendorf tubes, just after completion of FCPN synthesis. (WF)

3.2.3 MTT Assay

The viability of MG-63 cells, while being exposed with the developed FCPN, were assessed using MTT[3-(4, 5-dimethylthiazol-2-yl)-2, 5-diphenyl tetrazolium bromide] (SRL Pvt. Ltd., India) assay. This assay is based on the reduction of MTT to dark purple coloured formazan by mitochondrial succinate dehydrogenase which is soluble in organic solvent like Dimethyl sulfoxide (DMSO) (SRL Pvt. Ltd., India) and can be measured spectrophotometrically. Briefly, FCPN exposed cells were incubated for 3, 5, and 7 days, respectively. After respective incubation periods, the cells were washed with 1X phosphate buffer saline (PBS) and again incubated with 500 µL reconstituted MTT (5 mg/ml MTT in 1X PBS) and DMEM with 1:10 dilution for 6 hrs to form formazan crystals. The crystals were dissolved in DMSO and optical density was measured at 590 nm using ELISA microplate reader (BioradiMark^{TM}).

3.3 MALDI-MS. Bruker Daltonics (flexControl) Matrix assisted laser desorption ionization mechanism instrument was used with the matrix platform of sinapic acid. The sample was ionized with the pulsed nitrogen laser of 337 nm, followed by compilation of spectra in positive mode, with an average of 500 shots for each spectra. 1 ml of Matrix was prepared with 500 µl of 100% Acetonitrile, 500 µl of 100% Milli-Q Water (MQ), 1 µl of 0.1% Trifluoroacetic acid (TFA) and 10 mg of sinapic acid. The prepared matrix was stored for 7 days, 1 µl of the same matrix was used for spotting purpose. The ratio which was kept constant between the sample and the matrix was 1:1. 1 µl of matrix with 1 µl of sample was taken for spotting purpose.

3.4 Lifetime. Fluorescence lifetimes of the FCPN, BSA and Moringa leaf extract were measured with Edinburgh FL920 Fluorescence Life Time Spectrometer by Time Resolved Fluorescence Spectrometer (TRFS) technique. The samples were excited by the Laser and LEDs at wavelength of 375 nm and 496 nm, 598 nm, respectively. Fluorescence Lifetime decay spectra were acquired as far as 10,000 counts were laid-back. External circulating water bath was put into the lifetime decay setup to maintain the sample temperature at 25 °C.Tri- exponential fitting was performed on the lifetime-data to get the chi-square χ^2 (goodness of fitting) values close to 1.00 by GRG- Nonlinear solver.

3.5 Fluorescence Microscopy

The confocal microscopy was carried out using Carl Zeiss LSM 780 confocal microscope. The FCPN were exposed to cells for 24 hrs. Further, the culture media were aspirated off and cells were washed twice with 1X PBS. Following this, the fluorescent microscopic (Nikon eclipse LV100ND with Nikon DS-Qi2 camera) observation was carried out to study auto-fluorescence property of FCPN.

3.5.1 Corrected total cell fluorescence (CTCF) analysis

Corrected total cell fluorescence (CTCF) analysis was performed on Z- stacked images or shots of MG-63 cells acquired by confocal microscopy. The shots were acquired from bottom (0 μm) to top of the cell (22 μm) with total 12 number of slices (each slice of thickness ~1.8 μm). The details of CTCF analysis can be found elsewhere.[347]

3.5.2 Quantum Yield

The quantum yield of FCPN for green emission in water was calculated relative to the Rhodamine 6G, which is used as a standard fluorophore, its quantum yield is 0.92 in

water. The quantum yield of FCPN was evaluated by utilizing the following mathematical expression.

$$\varphi_{nc} = \varphi_r \frac{F_{nc} A_r \eta_{nc}^2}{F_r A_{nc} \eta_r^2} \quad (1)$$

In the above equation, φ = quantum yield, F = Integrated fluorescence intensity, A = Absorbance, nc = Nanocluster (FCPN) , r = Reference and η = refractive-index.

From fluorescence graph, we found: F_{nc}=31610650.15944, F_r =367458024.88005

Absorbance: A_{nc}= 0.09, A_r=0.02,

Refractive index: η_{nc}=1.33, η_r=1.33 and

Reference quantum yield φ_{std}=0.92.

Solvent: Water

Thus, The quantum yield of FCPN for green emission was calculated to be 0.0175 by eq. (1) with reference to quantum yield of Rhodamine 6G (0.92). (Figure 3.2)

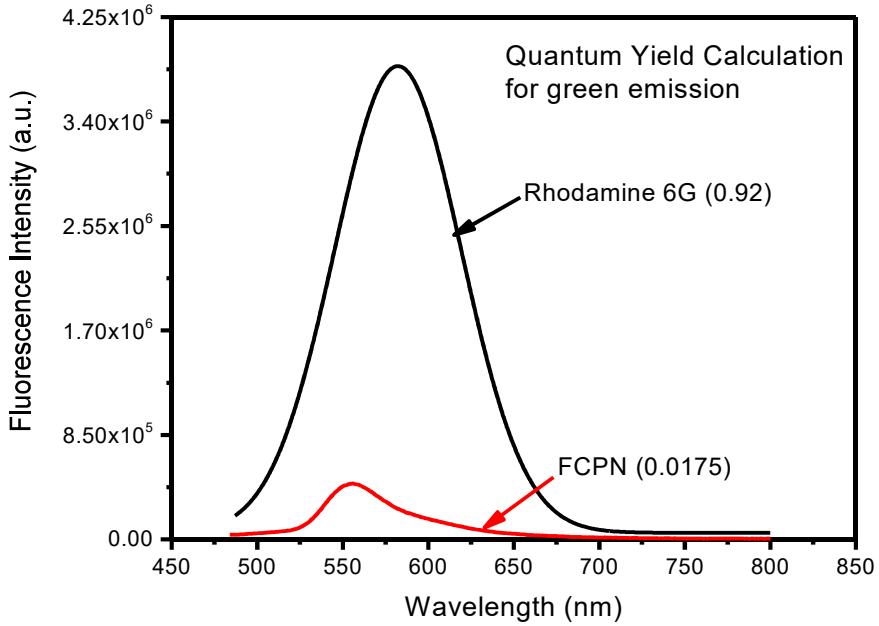

Figure 3.2 Fluorescence Spectra of FCPN against Rhodamine 6G for calculation of Quantum Yield of FCPN (green emission).

3.5.3 Quantitative methodology for determination of Nanocluster Concentration:

Method A: Based on TEM Data

Assumption:

Metal cluster is assumed to be spherical. Thus, cluster volume ($V_{cluster}$) is calculated by equation 1:

$$V_{cluster} = V_{atom} \times N \quad (1)$$

Where, V_{atom} is volume of atom and N is number of atoms present in one nanocluster.

Equation 1can be rearranged to give equation 2:

$$\left(\frac{4}{3}\right) \times \pi \times r_{cluster}^3 = N \times \left(\frac{4}{3}\right) \times \pi \times r_{atom}^3 \quad (2)$$

Where, $r_{cluster}$ is cluster radius obtained from TEM ($1.3/2 \sim 0.65$ nm) and r_{atom} is radius of calcium atom (180 pm). Thus equation 2 can be rearranged to calculate N:

$N = \left(\frac{r_{cluster}}{r_{atom}}\right)^3 = \left(\frac{0.65\times10^{-9}}{180\times10^{-12}}\right)^3 = 47$ atoms of calcium present in one nanocluster.

Single unit of FCPN contains 47 atoms of calcium.

Method B: Based on MALDI-MS Data

MALDI-MS analysis indicates that the maximum population of nanocluster (FCPN) constitutes of 50 calcium atoms. It can be noted that the numbers of atoms obtained from Method A and Method B are matching closely.

Calculation for concentration of nanocluster in solution:

50 ml of 10 mM aqueous $CaCl_2$ is used for nanocluster synthesis.

Number of moles of $CaCl_2 = 50\times 10 \times 10^{-3} = 0.5$

Number of calcium atoms in the precursor $= 0.5 \times 6.022 \times 10^{23} = 3.011 \times 10^{23}$

Thus, to calculate number of nanoclusters N_{NC} equation 3 is used, **Method A**:

$N_{NC} = \frac{N_{atom}}{N}$ (3)

$= \frac{3.011\times10^{23}}{47} = 6.406 \times 10^{21}$

Thus, 6.406×10^{21} nanoclusters are formed per 50 ml of $CaCl_2$

Answer: Thus, $\mathbf{1.281 \times 10^{20}}$ nanoclusters are formed per 1 ml of $CaCl_2$

Thus, to calculate number of nanoclusters N_{NC} equation 3 is used, **Method B**:

$N_{NC} = \frac{N_{atom}}{N} = \frac{3.011\times10^{23}}{50} = 6.022 \times 10^{21}$

Thus, 6.022×10^{21} nanoclusters are formed per 50 ml of $CaCl_2$

Answer: Thus, $\mathbf{1.204 \times 10^{20}}$ nanoclusters are formed per 1 ml of $CaCl_2$

*Hence the final concentration of the FCPN (i.e. **amount of nanoclusters**), was calculated by dividing N_{NC} by Avagadro's number N_A*

$$C_{NC} = \frac{N_{NC}}{N_A} = \frac{1.204 \times 10^{20}}{6.022 \times 10^{23}} = 2 \times 10^{-4}\ moles/ml$$

In FCPN powder, the concentration of nanocluster is measured to be 22.1 mg/ml.

Thus, Number of moles=0.5525

Number of nanoclusters in powder $= 0.5525 \times 6.022 \times 10^{23} = 3.327 \times 10^{23}$

$$C_{NC,powder} = \frac{N_{NC}}{N_A} = \frac{3.327 \times 10^{23}}{6.022 \times 10^{23}} = 0.55 \frac{moles}{ml\ of\ nanocluster\ solution}$$

3.6 Results and Discussion

The FCPN aqueous solution is dried in the oven at 80°C for 12 hrs and powder is ground to the fine powder for XPS and XRD analysis. For further applications and characterization such as TEM, fluorescence, life-time, MALD-MS, MTT, fluorescence imaging FCPN solution is used. The FCPN solution was drop-casted on the copper grid and microscopy was performed to estimate the size. Whereas, the powder sample was used to obtain the phase and crystallinity of the FCPN.

3.7 Characterization

3.7.1 Transmission Electron Microscopy (TEM) and XRD Analyses

The size of developed FCPN was determined using transmission electron microscopy. (Figure 3.3a). The TEM images are analysed for 150 nanoclusters, varying from 0.5-2 nm in size and size distribution was plotted by fitting Gaussian curve, as shown in Figure 3.3a. The size analysis was carried out using Image J software. The size distribution data indicated the formation of uniform sized ~1.3 ± 0.1 nm FCPN. Using the size analysis, approximately 47 Ca^0 atoms in the nanoclusters were calculated which closely matches with the number of atoms (50), predicted by the MALDI-MS (Section 3.5.3). Furthermore, the number of nanoclusters present/ml of solution using method TEM

analysis was found to be 5.628×10^{19}, while method based on MALDI-MS yielded this value to be 5.474×10^{19}, which is significantly close to each other. Whereas, number of nanoclusters in the powder were estimated to be 1.33×10^{23} using simple calculations. Using these calculation (Section 3.5.3), concentration of nanoclusters in the solution was also estimated to be $9.090 \times 10^{-5}\ moles/ml$ and that in powder was $0.22 \frac{moles}{ml\ of\ FCPN\ solution}$

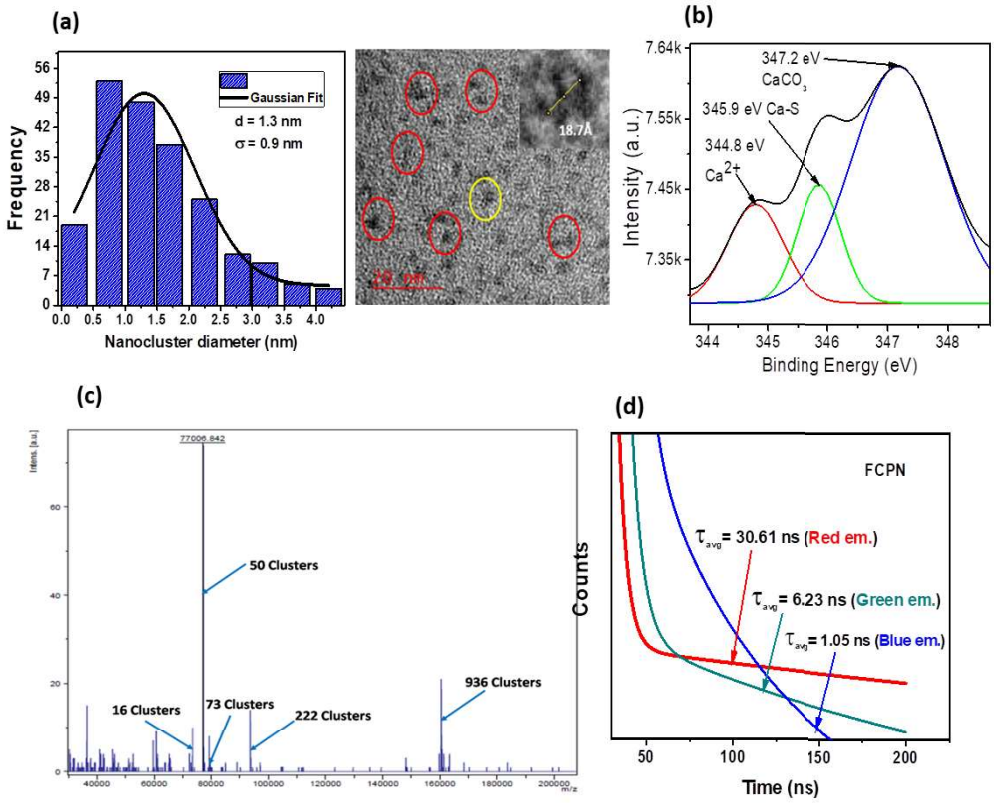

Figure 3.3 The FCPN (a) Size distribution and TEM image (b) XPS Spectra. (c) MALDI-MS spectra. (d) Comparitive fluorescence lifetime (model fitted) for red, green and blue emission of FCPN.

The dried FCPN powder is analyzed further for the phase formation and crystallinity using X-ray diffraction analysis [XRD, RigakuSmartLab 9kW Powder type (without χcradle), RIGAKU Corporation] .The XRD pattern (Figure 3.4a), shows the formation of the amorphous powder. A comparison with published reports, suggests the formation of nanoclusters.[109, 348] It has been reported that at the pre-nucleation stage, BSA protein further arrests the growth of the nanoclusters.[154]

After adding BSA protein (≈ 27 mg/ml at pH 10.7), a homogeneous transparent solution was collected (Figure 3.6c). As per TEM analysis, formation of small sized (~1.3 nm) nanoclusters comparble to the existing literature reports on $CaCO_3$ colloidal solutions are obtained. [349, 350]These nanoclusters can be assigned as pre-nucleation calcium carbonate ($CaCO_3$) nanoclusters. An earlier study has demonstrated that pre-nucleation nanoclusters are thermodynamically stable and exist as ion-clumps before the nucleation in the aqueous solution begins.[351]These findings also corroborate with the TEM findings of developed FCPN. The XRD results only revealed the amorphous nature of the FCPN. Since FCPN is ultra-small and constituted of few tens of atoms, XPS can easily provide information about surface chemistry, and elemental composition of FCPN with confidence.

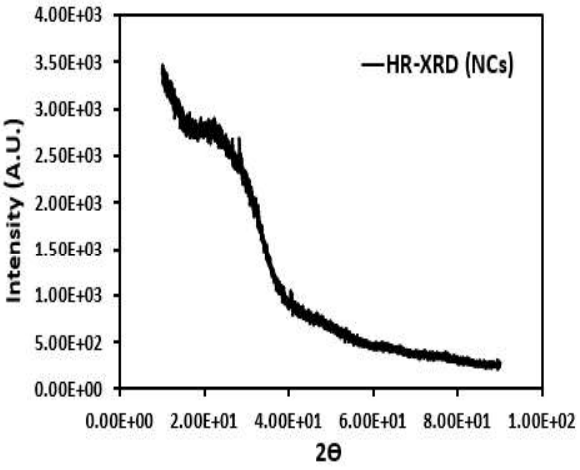

Figure 3.4a XRD of FCPN

3.7.2 XPS analysis of FCPN

Initially, XPS analysis (Amicus spectrometer) was carried out on dried M.oleifera leaf extract and the FCPN powder. All the peaks were adjusted as per the carbon peak (284.6 eV), as a reference, deconvoluted and interpreted. Initially, the XPS spectra of dry M.oleifera leaf extract shows O1s peak at the binding energy (B.E.) of 533 eV, indicating the presence of O^- the hydroxyl groups (Figure 3.5a),[352] endorsing ascorbic acid existence in the leaf extract. Furthermore, XPS spectra of leaf extract confirms the presence of free calcium (Ca^{2+}) indicated by the presence of $Ca2p_{3/2}$ and $Ca2p_{1/2}$ peaks at 347.6 eV and 350.9 eV, respectively (Figure 3.5b).[353-355] The XPS data for C1S in FCPN were deconvoluted to two peaks at 287.3 eV and 284.6 eV, corresponding to carbonates (CO_3^{2-})[356-358]and C-C bond[359], respectively (Figure 3.5c). It is important to notice that the XPS spectra of FCPN shows complete absence of (O1s) peak (Figure 3.6a), which indicates the complete utilization of ascorbic acid during the formation (Figure 3.4a and Figure 3.3b) of FCPN and large size $CaCO_3$ nanoparticles

(without BSA) (Figure 3.1). The disappearance of ascorbic acid and formation of FCPN is corroborated by O1s peak in FCPN at 532.3 eV[360] implying CO_3^{2-} due to the formation of $CaCO_3$[345] (Figure 3.5c). Furthermore, the $Ca2p_{3/2}$ peak of FCPN at 347.2 eV (Figure 3.3b) confirms the formation of $CaCO_3$[361-364]and the proposed hypothesis. The Ca2p peak at 345.9 eV suggest the formation of metal thiolate (Ca-S) bond between FCPN[365] and BSA, after reduction of Ca^{2+} ion to metallic calcium (Ca^0) [366], stabilizing ultrafine (~1.3 nm) FCPN (Figure 3.3b). Moreover, the Ca2p peak at 344.8 eV indicates the presence of free calcium (Ca^{2+}) ions in FCPN[367] (Figure 3.3b). The plausible reaction scheme for $CaCO_3$[345] nanoparticles and carbonate formation[368] at alkaline pH is provided as Figure 3.7. In essence, the XPS studies demonstrates the formation of FCPN with the use of M.oleifera leaf extract and BSA which supports the proposed design hypothesis. Next, emission/excitation of the FCPN and its control was ascertained by its fluorescence analyses.

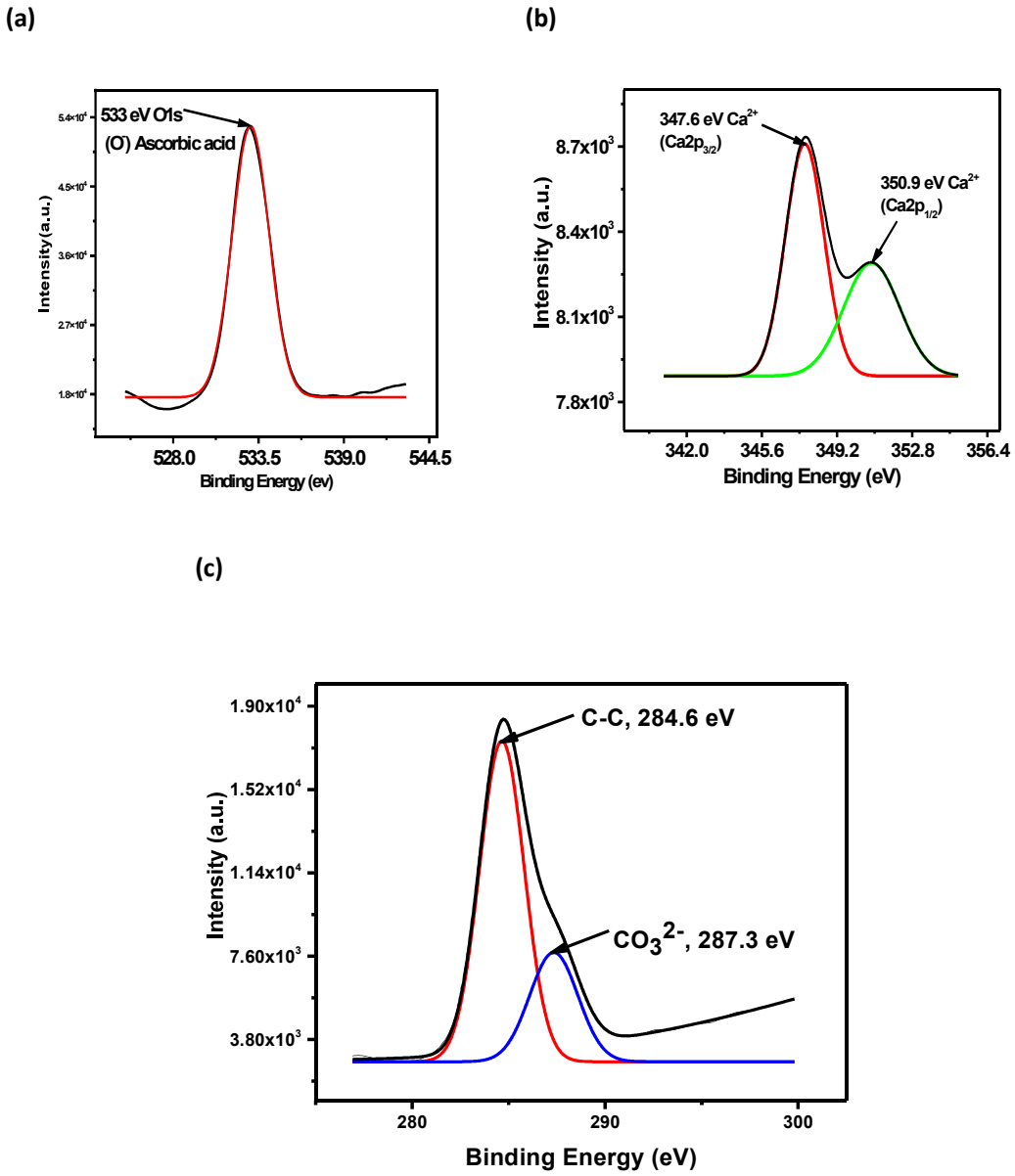

Figure 3.5 XPS spectra: M.oleifera leaf extract (a) O1s, peak at 533eV (b) $Ca2p_{3/2}$ and $Ca2p_{1/2}$ of free Ca^{2+} in M.oleifera leaf extract, peak at 347.6 eV and 350.9 eV. XPS spectra: FCPN (c) C1s of C-C, peak at 284.6 eV. (b) C1s of CO_3^{2-}, peak at 287.3 eV.

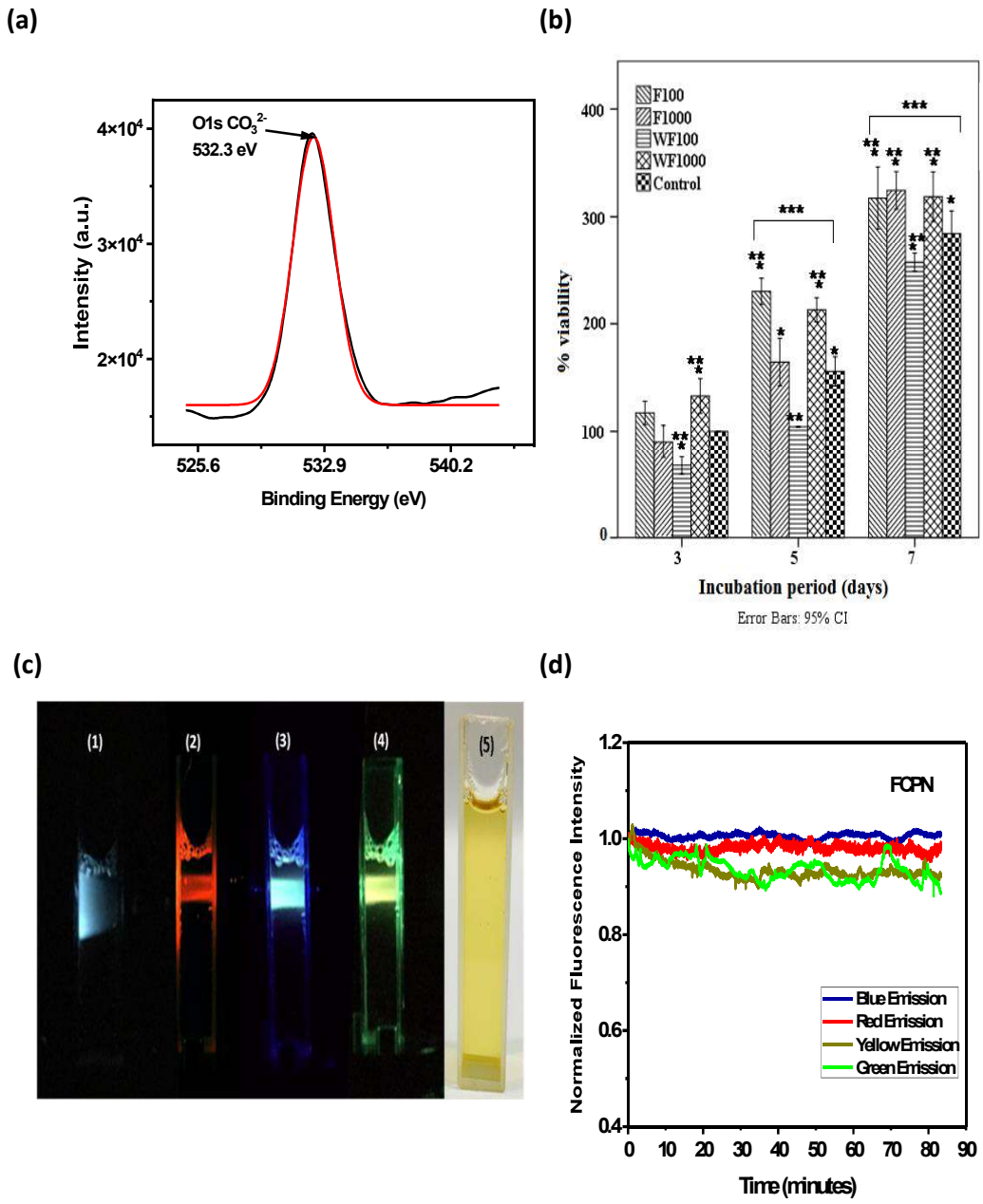

Figure 3.6 (a) XPS spectra (O1s) FCPN. (b) Time dependent viability of MG-63 cells against FCPN treatment. * indicates the statistical significant difference among the samples with respect to control, cultured for 3 days, ** indicates the statistical significant difference among the samples with respect to their respective control sample (culture media), and *** indicates the significant difference among the samples, incubated for 5 and 7 days with respect to those of 3 days ($P<0.05$)./ experiment repeated 3 times (c) Images of FCPN (1) Ex./Em 366 nm/Bluish white ,(2) Ex./Em. 595 nm /Red (3) (Ex./Em. 472 nm/ Green, (4) Ex./Em. 516 nm/Yellow) (5) Under sun light exposure. (d) Photostability of FCPN.

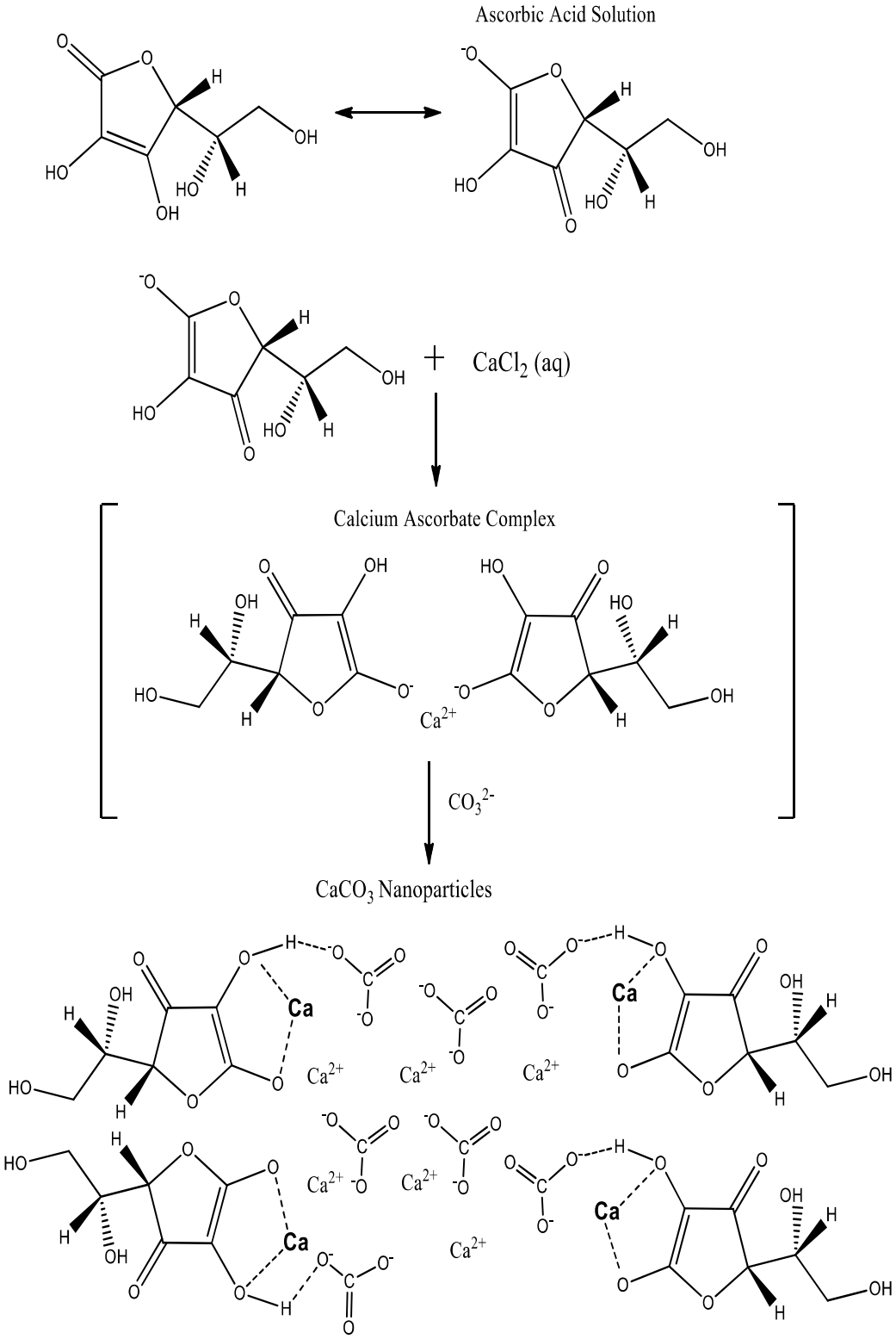
Ascorbic Acid Solution
CaCl2 (aq)
Calcium Ascorbate Complex
CO3 2-
CaCO3 Nanoparticles

$$CO_2\,(g) + 2NH_3\,(aq) \longrightarrow NH_2COO^-\,(aq) + NH_4^+\,(aq)$$

$$NH_2COO^-\,(aq) + NH_4^+\,(aq) + 2H_2O \longrightarrow NH_4HCO_3\,(aq) + NH_3.H_2O\,(aq)$$

$$NH_4HCO_3\,(aq) \rightleftharpoons HCO_3^-\,(aq) + NH_4^+\,(aq)$$

$$HCO_3^-(aq) + NH_3\,(aq) \rightleftharpoons CO_3^{2-}(aq) + NH_4^+(aq)$$

Figure 3.7 Reaction scheme.

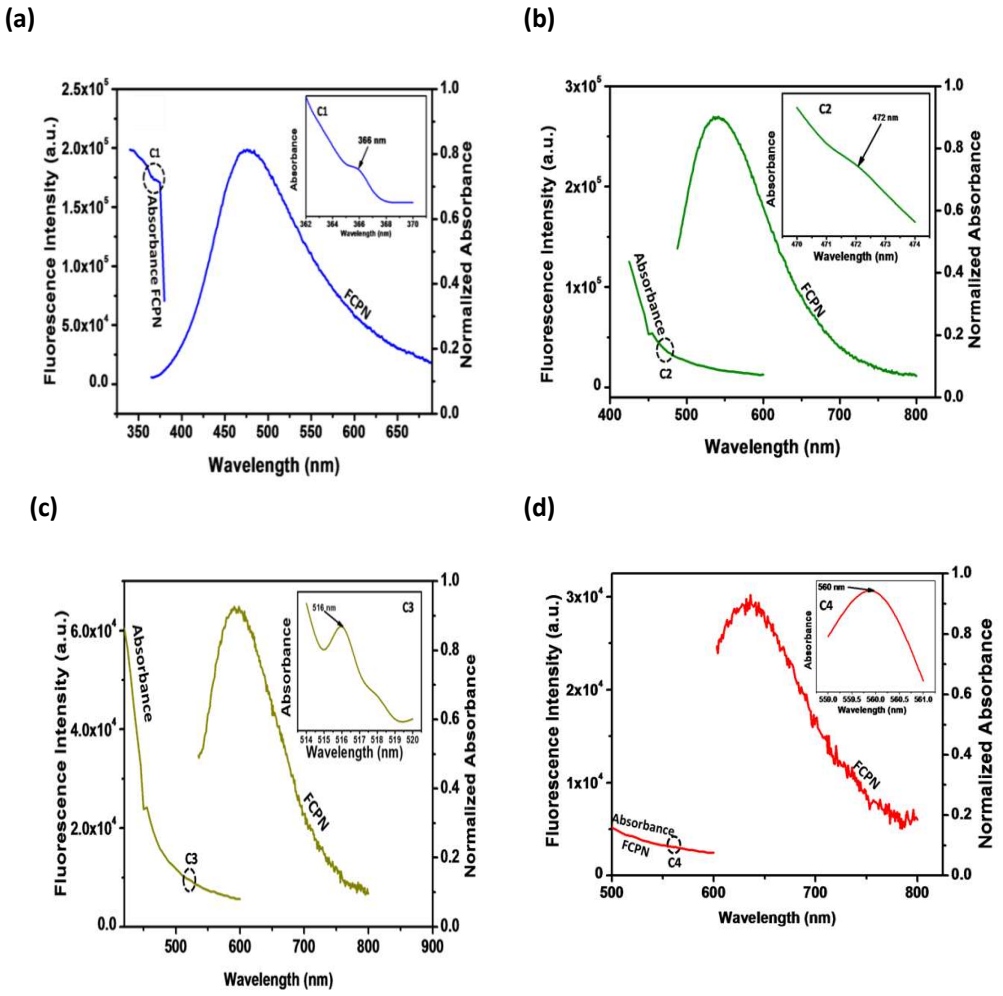

Figure 3.8 Fluorescence Spectra-FCPN: (a)-(Absorbance, C1) = 366 nm, λ_{exc}= 366 nm, λ_{em}=476 nm-blue). (b)-(Absorbance, C2 = 472 nm, λ_{exc} = 472 nm, λ_{em}=541 nm-green). (c)-(Absorbance, C3 = 516 nm, λ_{exc} = 516 nm, λ_{em}=595 nm-yellow). (d)-(Absorbance, C4 = 560 nm, λ_{exc} = 560 nm, λ_{em}=636 nm-red).

3.7.3 Fluorescence Characterization of FCPN

Next, the fluorescent properties (slit width = 2.6 nm) of the FCPN and control, were evaluated using PTI Quanta master 400 spectrofluorometer. (Figure 3.8 and Figure 3.9). Figure 3.8 shows that the absorbance wavelength of FCPN overlap with its excitation wavelength, in all the cases. Furthermore, at different excitations (366, 472, 516 and 560 nm), FCPN is observed to emit different colors viz. blue (476 nm), green (541 nm), yellow (595 nm) and red (636 nm) respectively (Figure 3.8). Further, Figure 3.9 displayed a strong fluorescence intensity from the FCPN as compared to its control sample, indicating fluorescence from FCPN, which is in line with the proposed design mechanism. Further, additional two controls- (i) without $CaCl_2$ (Control-B) and (ii) ascorbic acid (without leaf extract) (Control-C) were also prepared using conditions similar to FCPN synthesis. The fluorescence emission from these controls was compared with FCPN at different emission wavelengths and presented in Figure 3.9c. In the case of the first control, all constituents are present (except $CaCl_2$), it is observed that strong multicolour (477,541, 595 and 637 nm) emission from FCPN resulted as compared to the control. It is anticipated that the fluorescence emission from the control must be due to residual Ca^{2+} ions present in the leaf extract (confirmed by the XPS spectra $Ca2p_{3/2}$ and $Ca2p_{1/2}$ peak at 347.6 eV and 350.9 eV),[369] which might have resulted in the formation of FCPN in small quantities, and hence, noticable emission. Fluorescence studies performed on Control-C ($CaCl_2$, ascorbic acid, NH_4OH, NaOH and BSA) resulted in a strong multicolour (476 nm, 538 nm, 585 nm and 636 nm) emission as compared to FCPN (Figure 3.9b). This study established importance of ascorbic acid as reducing agent. Nevertheless, ascorbic acid present in the leaf extract not only excludes the external use of ascorbic acid but also reduces the additional optimization step, and reduces the time of synthesis, which is an added advantage over the FCPN synthesized

using pure ascorbic acid. Besides, fluorescence studies of Control-C also verifies that resulting fluorescence in the FCPN is not due to the plant extract. Next, the underlying mechanism, responsible for fluorescence in FCPN, UV-Visible spectroscopy was carried out.

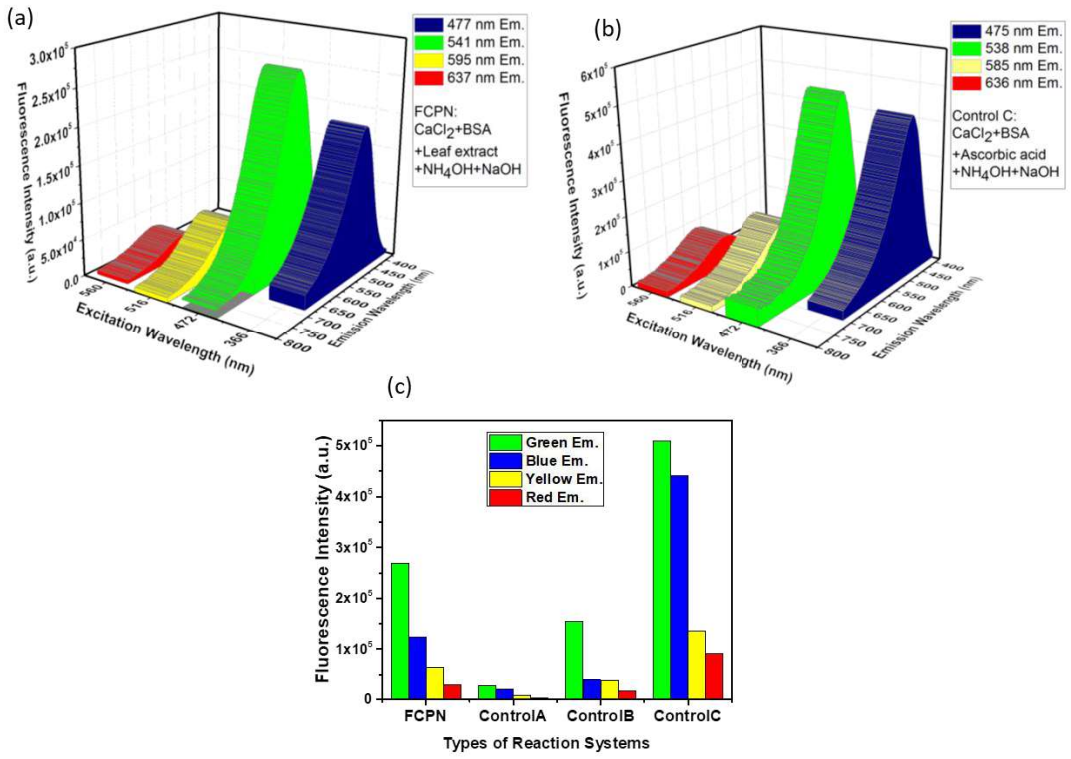

Figure 3.9 3D Fluorescence spectra: (a) FCPN (leaf extract) (b) Control C (pure ascorbic acid) (c) Comparative fluorescence intensity of FCPN, Control A, Control B and Control C at different excitations (Ex.) and emissions (Em.).

3.7.4 UV-Visible spectroscopic studies

The UV-Visible spectroscopic studies (Elico SL210 spectrophotometer) were performed on the FCPN, BSA and leaf extract, to understand the presence of bonds in FCPN. The UV-Visible absorption studies on BSA revealed an absorption peak at 280 nm (Figure 3.10), which is attributed to the amino acids (Tyr, Trp, and Phe). Such absorbance peak results due to the $\pi - \pi *$transition.[213] However, FCPN displayed two absorbance peaks at 282 and 292 nm[213], resulting from the shift in the $\pi - \pi *$ transition, which clearly suggests the formation of metal thiolate (Ca-S) bond in FCPN (Figure 3.10). These peaks (282 and 292 nm) are absent in BSA and M.oleifera leaf extract (Figure 3.11a and b). In addition to this study, a relatively soft ionization based technique-MALDI-MS, which produces small number of fragments and capable of analysing nanoclusters with higher m/z ratio (> 500,000) was used for analysis. Further, using MALDI-MS, size of the nanocluster core and its purity can be obtained. It provides number of atoms, involved in the formation of nanocluster, which can be further used for calculating number of nanoclusters in the solution and powder.

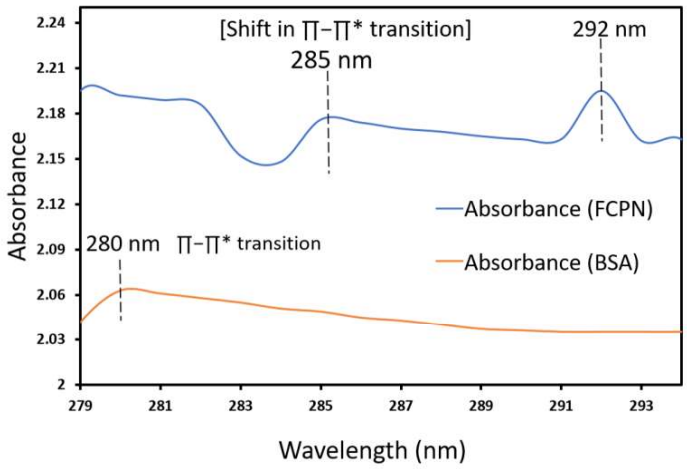

Figure 3.10 Absorption spectra: FCPN and BSA in the range from 279 to 293 nm.

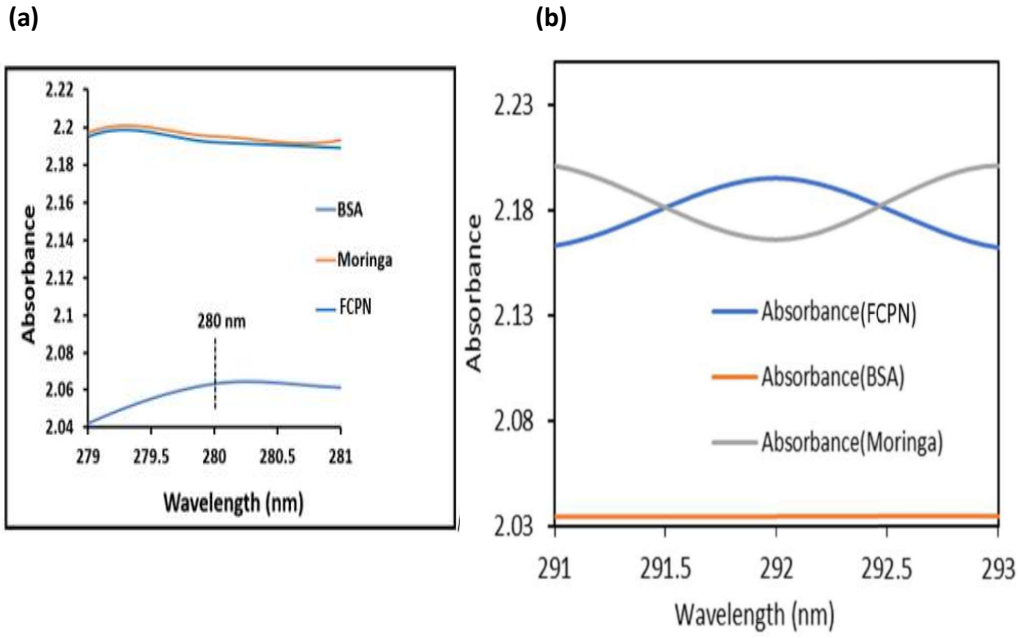

Figure 3.11 (a) FCPN, BSA and Moringa leaf extract in the range from 279 to 281 nm. (b) FCPN, BSA and Moringa leaf extract in the range from 291 to 293 nm.

3.7.5 MALDI-MS measurements

The number of FCPN molecular nanoclusters were further estimated by MALDI-MS measurements (MALDI-MS BrukerDaltonics (flex Control)). The MALDI-MS study was performed over FCPN, BSA and M.oleifera leaf extract are presented in Figure 3.3c and Figure 3.12a and b, respectively. The MALD-MS studies of BSA revealed a peak at m/z ratio of 66891 Da (Figure 3.12a) matching with actual molecular weight of BSA. The MALDI-MS of M.oleifera leaf extract studies revealed the proteins up to 5kDa molecular weight (Figure 3.12b). Similarly, MALDI-MS spectra for FCPN displayed peaks (Figure 3.3c) attributing to FCPN of sizes 16, 50, 73, 222 and 936 molecular nanoclusters. The peak at m/z value of 77006.8 was shifted by 10 kDa, indicating the formation of 77 kDa complex (largest intensity peak). This peak indicates the formation of FCPN having 50 molecular nanoclusters. This study suggests the formation of FCPN of varying

nanocluster sizes (16-936 atoms) with the major fraction belonging to 50 molecular nanoclusters. These polydispersity in sizes of nanoclusters, may corresponds to different emissions of 476, 541, 595, and 636 nm wavelength. However, further studies are required to establish a correlation between color emission and nanocluster size. Next, source of fluorescence emission in the FCPN was investigated using life time measurement. The life-time measurements provide distinct information about source of fluorescence (core or ligand charge transfer) and decay time of the FCPN. This information not only provides information about the active fluorescence mechanism but also provides some information about the fluorescence stability, crucial for its application in various areas.

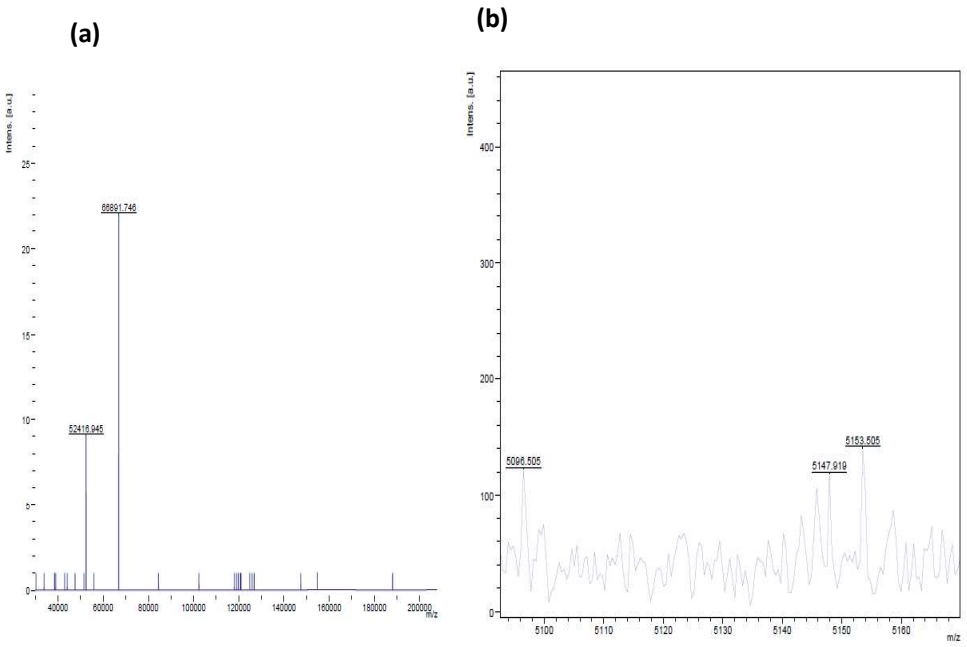

Figure 3.12 MALDI-MS spectra of (a) BSA, and (b) Moringa leaf Extract.

Table 1: Fluorescence lifetime of FCPN, BSA and leaf extract

System	α_1	τ_1(ns)	α_2	τ_2(ns)	α_3	τ_3(ns)	$\tau_{avg}{}^{a}$	χ^{2b}
Red-FCPN	0.0050	901.07	6.31	4.86	93.68	1.17	**30.61**	0.99
Green-FCPN	0.0089	276.8	5.14	6.44	94.84	1.5	**6.23**	1.01
Blue-FCPN	99.92	1.02	0.074	6.27	0.00014	83.22	**1.05**	1.30
BSA*	-	-	-	-	-	-	-	-
Leaf extract*	-	-	-	-	-	-	-	-
BSA**	98.36	0.82	1.63	4.66	0.0034	159.39	**2.13**	1.00
Leaf extract**	0.76	4.06	99.23	0.61	3	75	**0.98**	1.04
BSA***	0.26	7.28	99.73	1.28	0.0007	79.95	**1.40**	1.26
Leaf extract***	99.97	0.89	0.00004	85.33	0.023	5.67	**0.90**	1.27

'*' denotes excitation by 598 nm LED lamp with red emission, '**'denotes excitation by 496 nm LED lamp with yellow/green emission, '***'denotes excitation by 375 nm laser with blue emission,'$\tau_{avg}{}^{a}$' lifetime $\tau_{avg} = (\alpha_1\tau_1{}^2 + \alpha_2\tau_2{}^2 + \alpha_3\tau_3{}^2)/(\alpha_1\tau_1 + \alpha_2\tau_{2+}\alpha_3\tau_3)$,'$\chi^{2b}$' denotes extent of fitting among the model and experiment values.

3.7.6 Fluorescence Lifetime Analysis of FCPN

The lifetime measurements of FCPN, Moringa leaf extract, and BSA protein, were performed. Figure 3.13 shows the fluorescence lifetime decay curve. The lifetime measurements were carried out for different components (FCPN, BSA and leaf extract) (Table 1). The FCPN, BSA, and leaf extract displayed average lifetime of 1.05, 1.40, and

0.9 ns (Figure 3.13a b and c), respectively, for excitaton with blue light (375 nm). Similarly, for green excitation (496 nm), lifetime for FCPN, BSA and leaf extract were observed to be 6.23, 2.13, and 0.98 ns, respectively (Figure 3.13d e and f). However, for yellow excitation (598 nm), FCPN, BSA and leaf extract displayed a lifetime of 30.6, 0, and 0 ns, respectively, as shown in (Figure 3.13g h and i). The above observations suggest different underlying processes, responsible for fluorescence in each case. Early studies demonstrated fluorescence emission from a quantum-confined calcium sulphide nanoclusters (Ca-S), being an optical bandgap of 4.13 eV[370]. It is interesting to mention that, FCPN stabilized by metal thiolate bond (Ca-S) and emitting in the blue and green regions, also displayed an optical bandgap of ~4.16 eV (Figure 3.14). Similar observations were also reported by blue and green light-emitting BSA protected fluorescent magnesium nanoclusters (Mg-S)[213]. As shown in Figure 3.3d, it is important to notice that the average lifetime for FCPN, emitting in green (τ_{avg} =6.23 ns) and red regions (τ_{avg} =30.6 ns), is significantly higher than the autofluorescence lifetime (1-5 ns) for organic fluorophores[371, 372]

Furthermore, an earlier study has pointed out that both the metal to ligand charge transfer (MLCT) and LMCT (Ligand to metal charge transfer) phenomena are likely responsible for fluorescence in the complex between alkaline earth metals and ligands.[373] It is noteworthy that FCPN emission in the red region displayed average lifetimes of 30.6 ns (τ_1 = 910.7 ns, considered to be a long lifetime), which may be due to MLCT or LMCT mechanisms. In FCPN, the LMCT or MLCT mechanism comes into play via metal-thiolate bond (Ca-S) interaction. The metal-thiolate (Au-S) bond of the fluorescent gold nanocluster [big clusters size (Au_{25})] played an important role during the charge transfer from ligand to the metal core (LMCT). The LMCT resulted in a long lifetime (≈ 0.5-1.2

μs) and red emission[222] from the gold nanoclusters. Furthermore, the formation of different sizes FCPN may show different colour emission, due to polydispersity in

size (Figure 3.15). The multicolor fluorescent emission were also observed in MoS_2 as well as functionalized quantum dots, based on polydispersity in sizes.[374, 375]The formation of different size FCPN has been indicated by the MALDI-MS (Figure 3.3c) and TEM studies, as shown in Figure 3.3a. The short lifetimes (τ_{avg}=1.05 ns and τ_{avg}=6.23 ns) from the blue and green- emitting FCPN, respectively may result from metal core, due to the size-confinement.

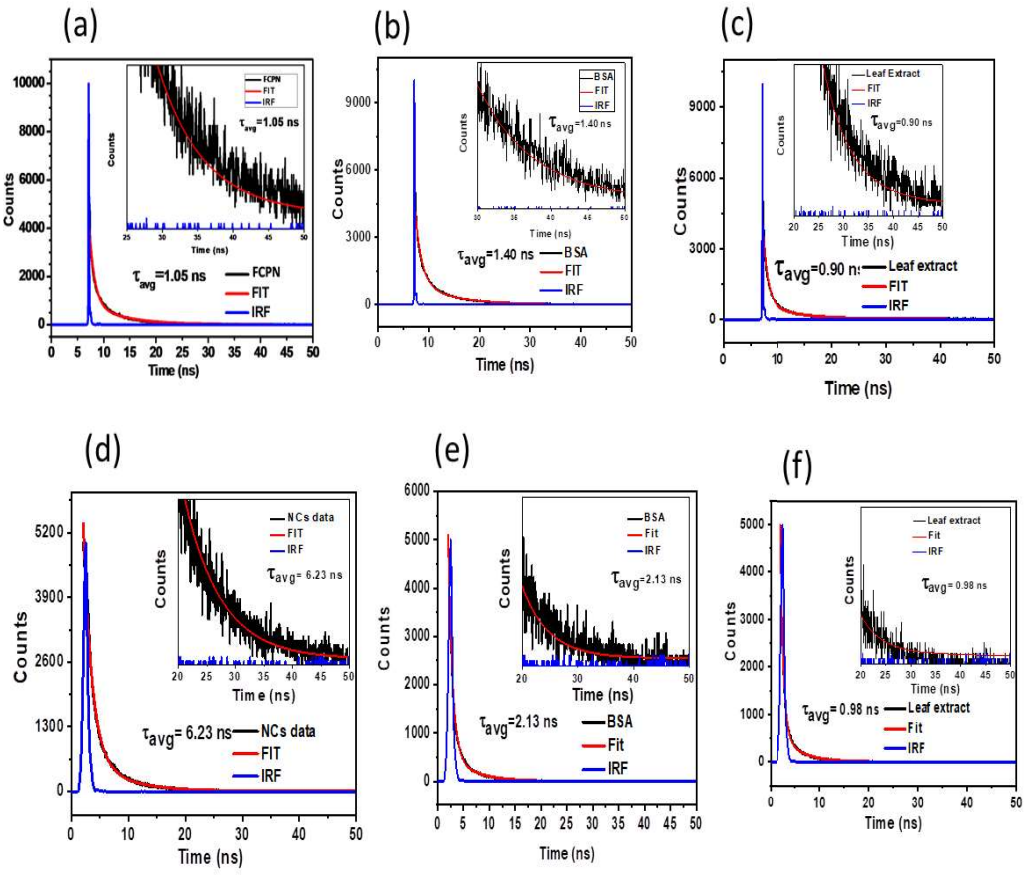

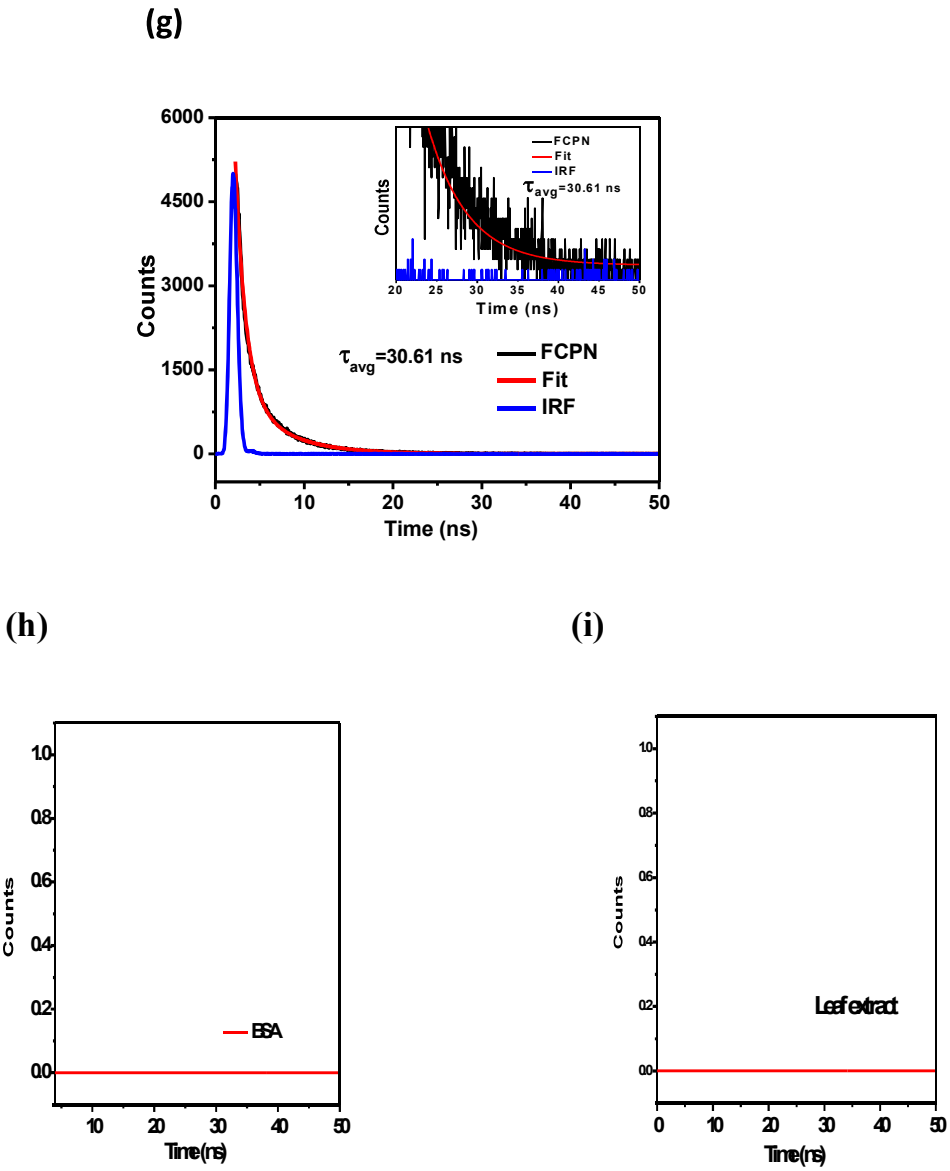

Figure 3.13 Fluorescence lifetime (FL) spectra of (a) FCPN (b) BSA Protein (c) leaf extract, with ex/em 375/485 nm; FL spectra of (d) FCPN (e) BSA protein (f) leaf extract with ex/em of 496/565 nm, using LED lamp as excitation source; FL Spectra of (g) FCPN (h) BSA Protein (i) leaf extract, with ex/em of 598/674 nm, using LED lamp as excitation source; All of the above images contains inset figure showing the zoomed images of the same curve.

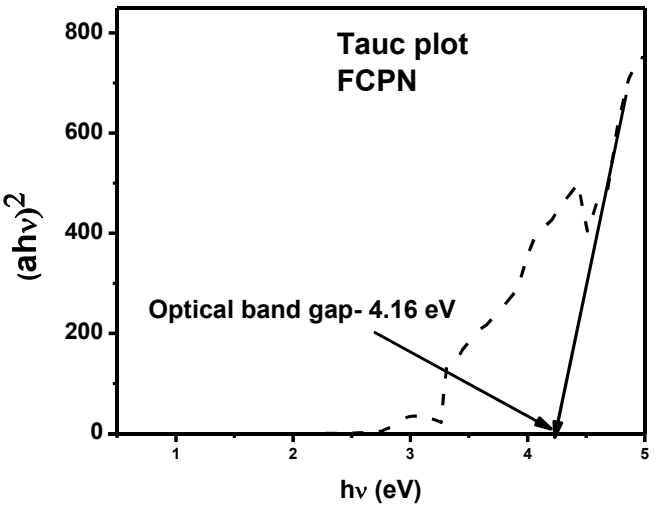

Figure 3.14 Band energy gap for FCPN.

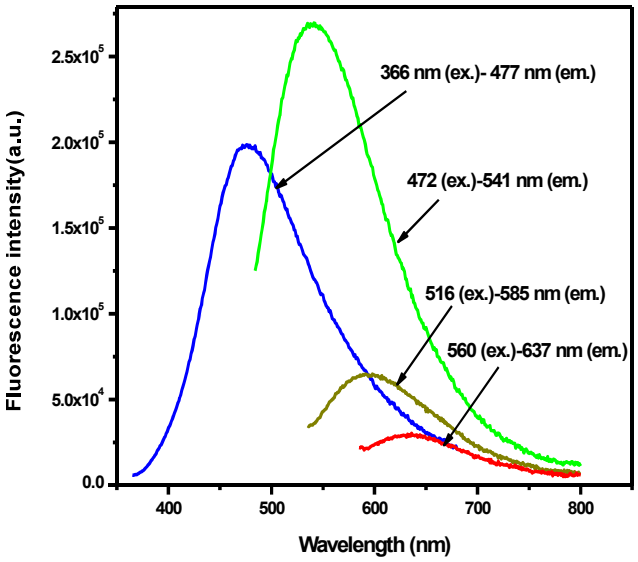

Figure 3.15 Fluorescence spectra of FCPN under different excitations (ex.) and different emissions (em.).

3.7.7 FTIR analysis of FCPN

The functional groups and bonds formed during the synthesis, were studied using Fourier transformed infrared spectroscopy (FTIR-Nicolet iS5, THERMO Electron Scientific Instruments LLC). The FTIR spectra for the BSA, and FCPN are presented in (Figure 3.16). The spectra for BSA protein comprised of amide I (1651 cm^{-1}), amide II (1536 cm^{-1}) and amide III bands (1239 cm^{-1}). These bands were associated with C=O stretch (1600-1700 cm^{-1}), C-N stretch coupled with N-H (1480-1575 cm^{-1}), and C=O bend coupled with C=C stretching (1229-1301 cm^{-1}), respectively. The bands at 2955 and 3306 cm^{-1} in BSA, are attributed to C-H and O-H/N-H stretch, respectively.[376, 377] The FTIR spectra of FCPN and BSA were compared together, as shown in Figure 3.16a. A comparative analysis revealed the decreased intensity of amide I (1651 cm^{-1}), amide II (1536cm^{-1}), amide III (1239 cm^{-1}), and O-H/N-H stretch (3306 cm^{-1}) for the FCPN, as compared to

BSA. As per early reports, the reduction in the amide I, II and III and O-H/N-H stretch peaks are known to occur during nanocluster formation.[111, 377] Furthermore, FTIR spectra for BSA revealed a weak peak at 2368 cm^{-1} (Figure 3.16b) of enlarged image indicating the presence of free S-H bond in the protein[378], which disappears, on the formation of FCPN, supporting the formation of metal-thiolate bond (Ca-S), also corroborated by the XPS and UV-Visible studies (Ca 2p peak at 345.9 eV).The formation of a metal-thiolate bond also ensures the capping of FCPN by the BSA protein. Furthermore, the FTIR studies show a tiny weak peak at 2363 cm^{-1} indicating the absorption of CO_2 from the atmosphere[379, 380], which probably facilitates the formation of carbonate (Figure 3.16b). The addition of NaOH facilitated CO_2 absorption[381] and drove the reaction to completion.

3.8 Design Rational of FCPN

The fluorescent nanoclusters with high cellular uptake, high photostability, low toxicity, eminent water dispersibility, high biocompatibility and low cost of synthesis are highly desirable, which is inline with the properties of synthesized FCPN. Besides, the decomposition products of $CaCO_3$ are water soluble and can be easily excluded from the body.[335-337]Despite high reactivity of magnesium and calcium, the synthesis of fluorescent BSA protected magnesium clusters (Mg-S)[213] paves the way for the development of fluorescent, BSA capped $CaCO_3$ prenucleation nanoclusters (FCPN). For such synthesis, M.oleifera leaf extract is used as a natural source of ascorbic acid.[342] The presence of ascorbic acid is confirmed by XPS analysis, as shown in Figure 3.5a. To restrict the size of the $CaCO_3$ and prevent it from dissolving into the solution, non-toxic, inexpensive and readily available, BSA[254, 342]protein was used as a capping and stabilizing agent. The proposed reaction mechanism for $CaCO_3$ nanoparticle formation by

ascorbic acid[345]is shown in Figure 3.7.The reaction was carried out at the basic pH (10.7), which was maintained by the addition of NaOH (1 M) solution. The addition of NaOH facilitated CO_2 absorption[381] and drove the reaction to completion. The synthesis of the resulting nanocluster was confirmed to constitute $CaCO_3$ by the XPS results (Figure 3.3b). Further, XPS analysis confrmed metal-thiolate (Ca-S) association between $CaCO_3$ prenucleation clusters and thiolate (-S-H) of BSA, confirming capping of the nancolusters by the protein molecules (Figure 3.3b). The fluorescence emission from these nanoclusters was ascertained by fluorescence (Figure 3.9) and its life-time measurements (Figure 3.3d and Figure 3.13). Furthermore, the electron microscopy results verified the formation of very small $CaCO_3$ prenucleation nanoclusters, as shown in Figure 3.3a. Additionally, lifetime measurements verified the origin of fluorescence in the nanoclusters as core of the $CaCO_3$ and LMCT/MLCT mechanisms, as discussed in the above sections. The detailed characterization of the prepared fluorescent nanoclusters strongly supported the proposed design hypothesis.

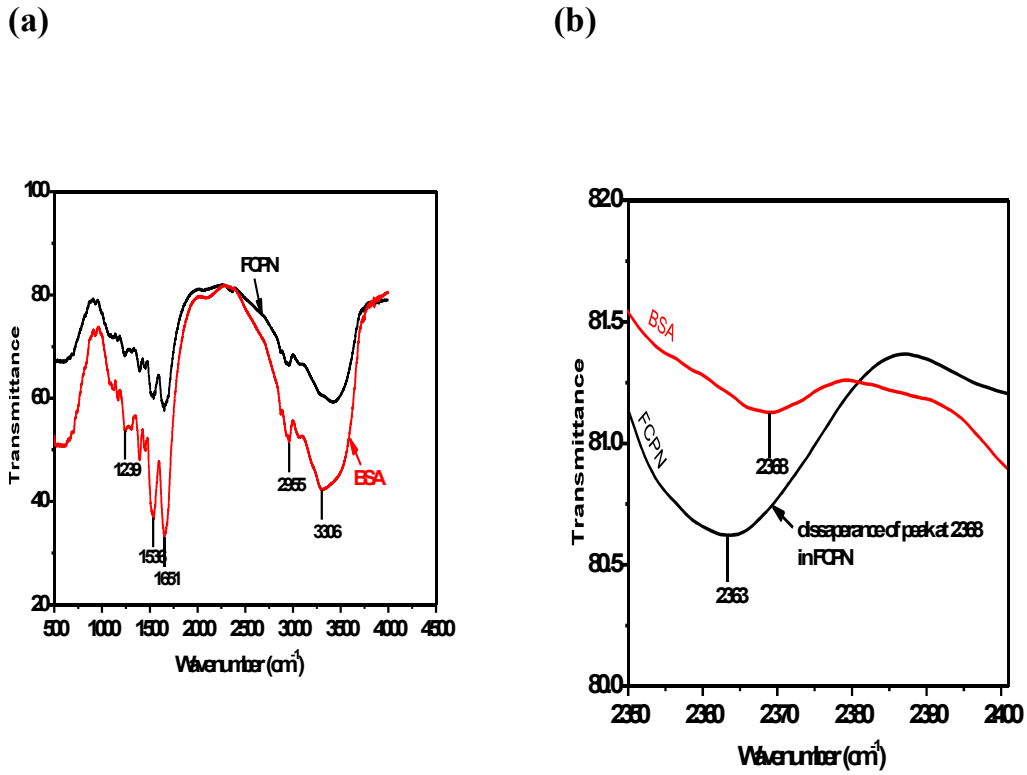

Figure 3.16 FTIR spectra: (a) FCPN and BSA, (b) zoomed image of FCPN and BSA in the range varying from 2300 cm^{-1} to 2400 cm^{-1}.

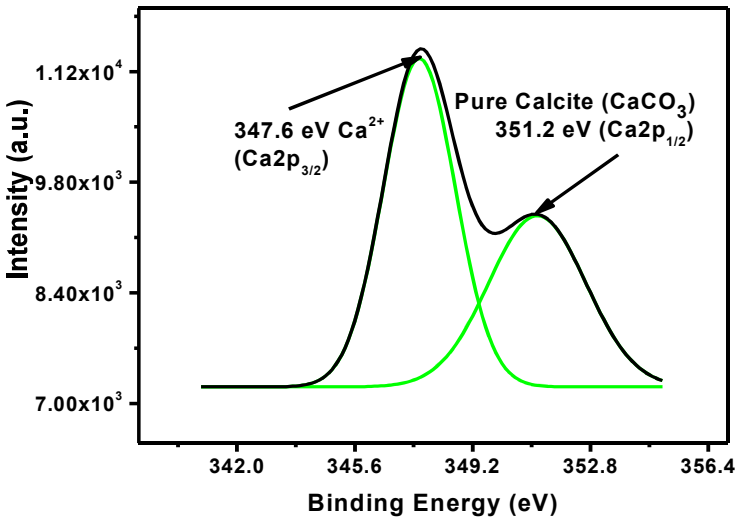

Figure 3.17 XPS spectra: large size $CaCO_3$ Nanoparticles (NP'S) ~49 nm (Control A). (a) $Ca2p_{3/2}$ of Ca^{2+}, peak at 347.6 eV. (b) $Ca2p_{1/2}$ of pure calcite crystal, peak at 351.2 eV.

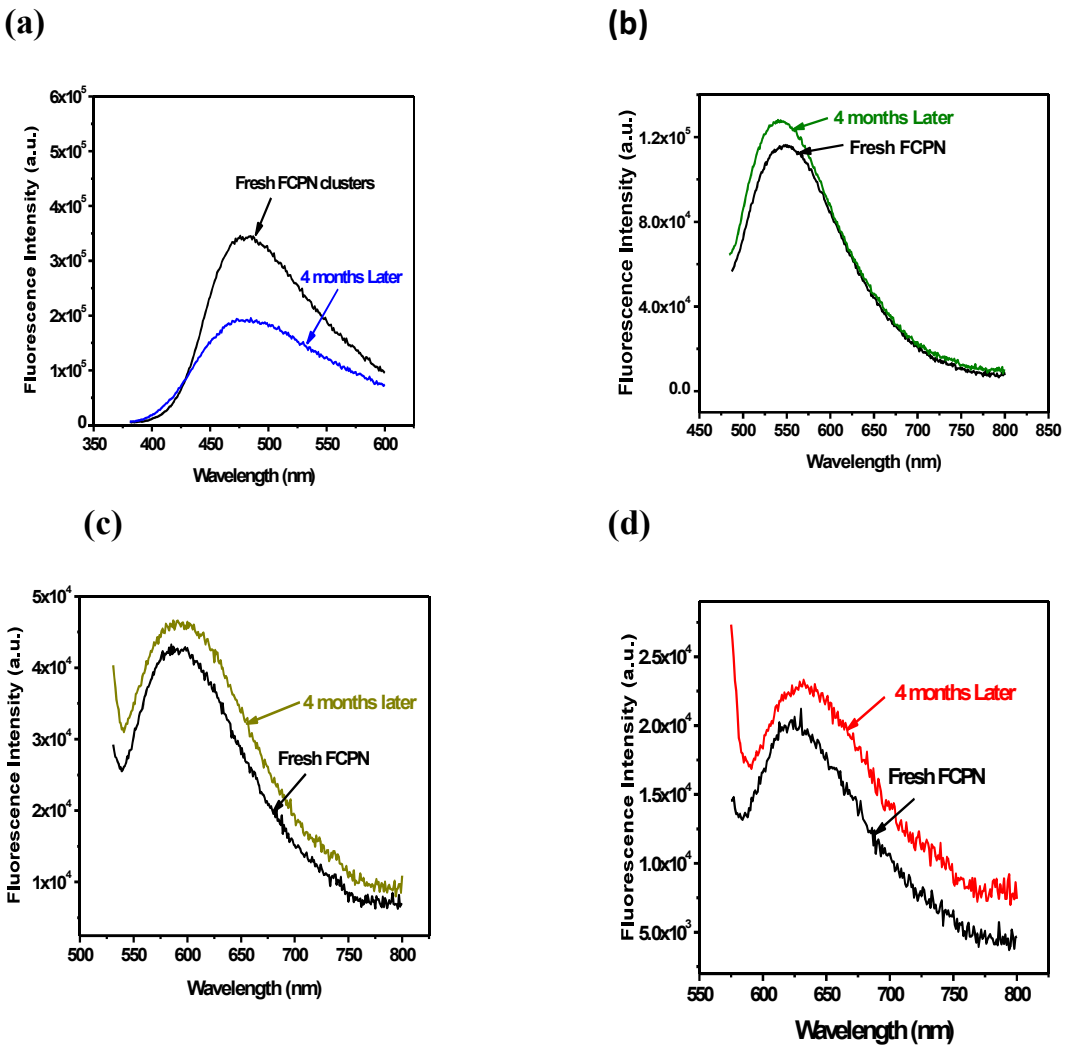

Figure 3.18 Fluorescence stability of FCPN over a period of time (4 months) at: (a) Ex. 366 nm, Em. 477 nm, (b) Ex. 472 nm, Em. 541 nm, (c) Ex. 516, Em. 595 nm (d) Ex. 560 nm, Em. 636 nm.

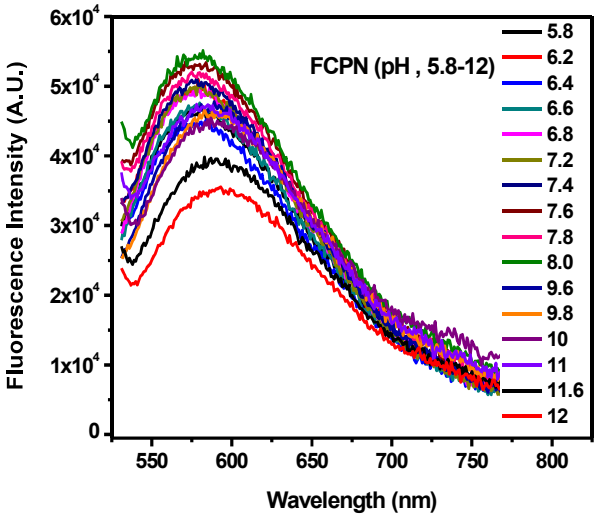

Figure 3.19 pH stability of FCPN at different pH, ranging from 5.8 to 12.

3.9 Optimization of Synthesis Procedure for FCPN

The concentrations of $CaCl_2$ and BSA precursors were crucial during FCPN synthesis. Initially, $CaCl_2$ concentration was fixed at 10 mM and the sufficient amount of BSA (~27 mg/ml) protein, ensuring complete FCPN protection by BSA protein, was taken. The optimization studies revealed that with decrease in the concentration of BSA protein to ~0 mg/ml, while keeping the concentration of $CaCl_2$ precursor constant (10 mM), results in an increase in the size of $CaCO_3$ nanoparticles (~49±10 nm) with no fluorescence (Figure 3.1) and (Figure 3.9c), which was synthesized by using leaf extract of Moringa oleifera, containing ascorbic acid. The XPS studies of non-fluorescent large $CaCO_3$ nanoparticles (~49 nm) reveal that $Ca2p_{1/2}$ peak at the B.E. of 351.2 eV, suggesting the formation of pure calcite crystal with presence of Ca^{2+} also (347.6 eV, $Ca2p_{3/2}$) (Figure 3.17)[353, 382].Such dependence of fluorescence on the $CaCO_3$ size is likely due to the quantum confinement effect. The FCPN is, therefore, synthesized using high concentration of BSA (~27 mg/ml).The prolonged use of FCPN in bioimaging requires photostability evaluation, which is discussed below.

3.10 Application of FCPN

3.10.1 FCPN Photostability

The Photostability of FCPN plays an important role in fluorescence imaging. During fluorescence imaging, the fluorophore embedded in the tissue/cell are exposed to strong light source for prolonged period of time. This may results in permanent or temporary loss of FCPN fluorescence and therefore, photostability experiments are required. The FCPN photostability studies were performed by exposing the colloidal solution for 83 min with different (476, 541, 595, and 636 nm) emissions. The time-dependent studies revealed no significant drop (~10% drop) in the emission intensity, even after prolonged (83 min) exposure to the strong light source (Figure 3.6d). Furthermore, FCPN photostability was also performed as a function of its shelf-life. The FCPN was stored at 6°C for 4 months, and the change in emission intensities (476, 541, 595 and 636 nm) were acquired. The shelf-life studies demonstrated a slight decrease in blue intensity, which was compensated by the minor increase in fluorescent intensity in green, yellow and red regions (Figure 3.18a b c and d). However, a slight increase in the red-intensity after a certain interval, may suggest slight aggregations. Briefly, synthesized FCPN can be considered as photostable for a reasonable period of storage time. Furthermore, variation in FCPN fluorescence intensity as a function of pH change (5.8-12) was evaluated for yellow emission (595 nm), which demonstrated no significant drop (Figure 3.19). Furthermore, for the biological application of FCPN, cellular viability experiments were carried out.

3.10.2 MTT Assay

To estimate the FCPN cytocompatibility, 3-(4,5-dimethylthiazol-2-yl)-2,5-diphenyl tetrazolium bromide (MTT) test was performed. The validity assay was performed for

filtered (F) and non-filtered (WF) FCPN at (1/100, 1/1000) dilution of the stock solution (22 mg/mL). Figure 3.6b shows MTT assay results in terms of percentage cell viability for control (culture media) as well as FCPN treated cells, which was incubated for 3, 5, and 7 days. The increased value of cellular viability reflects the increase in cells proliferation within the stipulated incubation period. The statistical analysis suggest that the viability of cells, incubated for 5 and 7 days increases significantly with respect to those of 3 days. Also, for the similar incubation period, statistical significant difference in viability has been seen for FCPN treated cells as compared to control (culture media) sample. It can be seen from Figure 3.6b that, all the examined concentrations of FCPN highly supports cells proliferation except WF100. To assess the viability of FCPN as the fluorescent imaging agent, fluorescence microscopy was performed.

3.10.3 Fluorescence Microscopy

Multicolor fluorescent cellular imaging (Nikon eclipse LV100ND) of MG-63 cells was performed using FCPN as a bioimaging agent. Figure 3.20 (a b c and d) shows the fluorescent images of MG-63 cells, incubated with the FCPN, as well as for the control (culture media) (Figure 3.24). Fluorescence images were acquired in green, blue, yellow and red colour. The control images (MG-63 cells without FCPN and with culture media) show no fluorescence emission in the blue, green, yellow and red color, indicating no autofluorescence from the cells (Figure 3.24a, b, c and d). The MG-63 cells incubated with the FCPN displayed uniformly stained fluorescence images in blue, green, yellow and red color. The colored images, when superimposed, yielded white image (Figure 3.20e). The MG-63 cells incubated with the FCPN were also used to obtain bright-field image (Figure 3.20f). Under excitation by different light source, FCPN showed multicolour emission (Figure 3.6c 1, 2, 3 and 4). FCPN, under sun light exposure, is also shown as Figure 3.6c (5). Next, internalization of FCPN and its penetration capability

inside the MG-63 cells was ascertained using CTCF analysis, performed over the confocal images. The CTCF analysis provides the change in the FCPN emission intensity with the finite depth of penetration within the cells, enabling penetration measurements and its localization within the cells.

3.10.4 CTCF Analysis & Effect of Cluster Size

The confocal images are acquired for FCPN exposed MG-63 cells and control (culture media). The fluorescence activity was monitored on 12 slices from bottom (0 μm) to the top of the cell (22 μm). Here, 0 μm corresponds to the lower cell surface and 22 μm corresponds to the top of the cell surface. [Figure 3.21 and Figure 3.25 (1)] represent Z-stack confocal cell images (12 shots) of MG-63 cells, incubated with FCPN emitting in blue region (Ex. 366 nm, Em. Blue), and mean fluorescence intensity graph, respectively. The maximum fluorescent intensity (100%) was observed at 16 μm above the lower cell surface (0 μm), indicating the efficient uptake of the FCPN by the cell lines. While at the bottom cell surface (0 μm), the fluorescent intensity was observed to be 21.79% of maximum fluorescent intensity, suggesting entire fluorescence from the bulk of the cell body. For the blue emitting FCPN, pattern corresponding to the cell mean fluorescent intensity percentage was found to be as follows: (a)=21.79%, (b)=32.95%, (c)=44.25%, (d)=58.09%, (e)=70.87%, (f)=86.73%, (g)=93.84%, (h)=97.11%, (i)=100%, (j)=76.02%, (k)=57.12%, (l)=45.64%. Similar evaluation was carried on MG-63 cells, exposed with FCPN, emitting in the green region. In case of green emitting FCPN, the bottom of the cell surface (0 μm) displayed 18.25% of maximum fluorescent intensity, suggesting the uptake of FCPN by MG-63 cells, due to which fluorescence from the surface of the cell appears close to the background. Briefly, green emitting FCPN . [Figure 3.22 and Figure 3.25 (2)] the cell mean fluorescent intensity percentage pattern were as follows: (a)=18.25%, (b)=30.74%, (c)=44.35%, (d)=41.76%, (e)=53.49%, (f)=71.35%,

(g)=73.58%, (h)=75.67%, (i)=100%, (j)=90.83%, (k)=70.86%, (l)=50.99%. Although, in the case of MG-63 cells, exposed with FCPN, the images represent red fluorescence. [Figure 3.23 and Figure 3.25 (3)]The fluorescent intensity at the bottom of the cell surface was found to be 15.96% of maximum value. The pattern corresponding to the cell mean fluorescent intensity percentage were as follows: (a)=15.96%, (b)=18.76%, (c)=28.54%, (d)=37.06%, (e)=38.95%, (f)=45.34%, (g)=57.09%, (h)=71.60%, (i)=89.58%, (j)=100%, (k)=53.71%, (l)=48.47%. The pattern (m) corresponds to control (culture media) showing no emission in blue, green and red region when excited at 366 nm, 472 nm and 472 nm, respectively. In this case, maximum fluorescent intensity (100%) was observed at 18 μm above the bottom of the cell surface.

On comparison, it is observed that blue and green emission from the MG-63 cells have same slice locations suggesting that both, blue and green FCPN remains spatially confined at the same depth (i=16 μm). These slice stacks indicate that blue and green emitting FCPN have traversed (22-16 = 6 μm) 6 μm from the top of the cell, making a 2-D slice, as shown in the Figure 3.21 3.22 and 3.23 and Figure 3.25 (1 2 and 3). However, in case of MG-63 cells, exposed with red emitting FCPN, the intense red emission was colocalized at 4 μm (22-18 μm) from top of the cell. This indicates that small FCPN nanoclusters (blue and green FCPN) diffused in larger cross-section of cell as compared to the red emitting FCPN. Such localization of certain population of FCPN at different places in cells suggest the formation of different size nanoclusters. Further, multicolor emission from the FCPN from different penetration depths, might have resulted due to this size effects. This observation is also in line with that of the MALDI-MS observations. As discussed already, MALDI-MS shows different peaks, which represents the existence of different subpopulations of FCPN.

Additionally, the viability (100%) of cells on FCPN was found to be better than fluorescent gold[383] (~85-90%) and magnesium nanoclusters (Mg-S)[213] (~95%). On contrary, some of the organic dyes such as, Alexa Fluor were found to be reasonably toxic, precluding its clinical usage[384]. Moreover, FCPN displayed far better photostability than Alexa Fluor,[385, 386] which is advantageous for the cell-imaging applications. While blue-emitting gold nanoclusters displayed poor photostability as compared to FCPN. The photostability of FCPN in green and blue region was found to be comparable to gold nanoclusters.[71] Interestingly, the lifetime of FCPN in green and red regions was found to be 6.23 ns and 30.6 ns, respectively, which is longer than that of cell auto-fluorescence (2−5 ns)[387]. The long lifetime of FCPN would allow auto fluorescence-free lifetime imaging of cells. On contrary, short-lived (τ_{avg} = 3.4 ns) Alexa Fluor-488[387] is not fit for lifetime imaging due to poor signal to noise ratio. Whereas, gold nanoclusters reveal the fluorescence lifetime in the range of 0.5 ns [383](green emission) to 100 ns (red emission) or higher[388].

Indeed, Alexa Fluor displays higher quantum yield (~0.66) as compared to FCPN (~0.0175 relative to Rhodamine 6G = 0.90±0.2)[389, 390](Figure 3.2). Although, the relative quantum yield of the developed FCPN is higher as compared to fluorescent gold clusters (~0.012).[383] Despite of excellent quantum yield and multicolor emission by Alexa Fluor, its synthesis is very complex and multistep process.[391] In addition, for different color emission, separate synthetic routes are used. On the other hand, multicolour FCPN uses green synthesis route, which is inexpensive and one-pot synthesis. Further, multicolour emission by FCPN makes it far better imaging tool as compared to highly expensive[392] organic dye Alexa Fluor.

The FCPN (~1.3 nm) is comparable in Alexa Fluor size (~0.4 nm),[393] but smaller than gold (~2.6 ± 0.7 nm)[383] and magnesium nanoclusters (8.5 nm)[213]. Furthermore,

FCPN is stable in pH rnaging from 5.8-12, which is as good as Alexa Fluor dye (4-10)[393], fluorescent gold (5-12.5)[394] and magnesium clusters[213]. Besides, FCPN shelf life is 4 months which is comparable to fluorescent gold[395] and magnesium[213] nanoclusters (Table 2). It can, therefore, be concluded that FCPN has a huge potential as a novel tool for cell imaging application and nanomedicine.

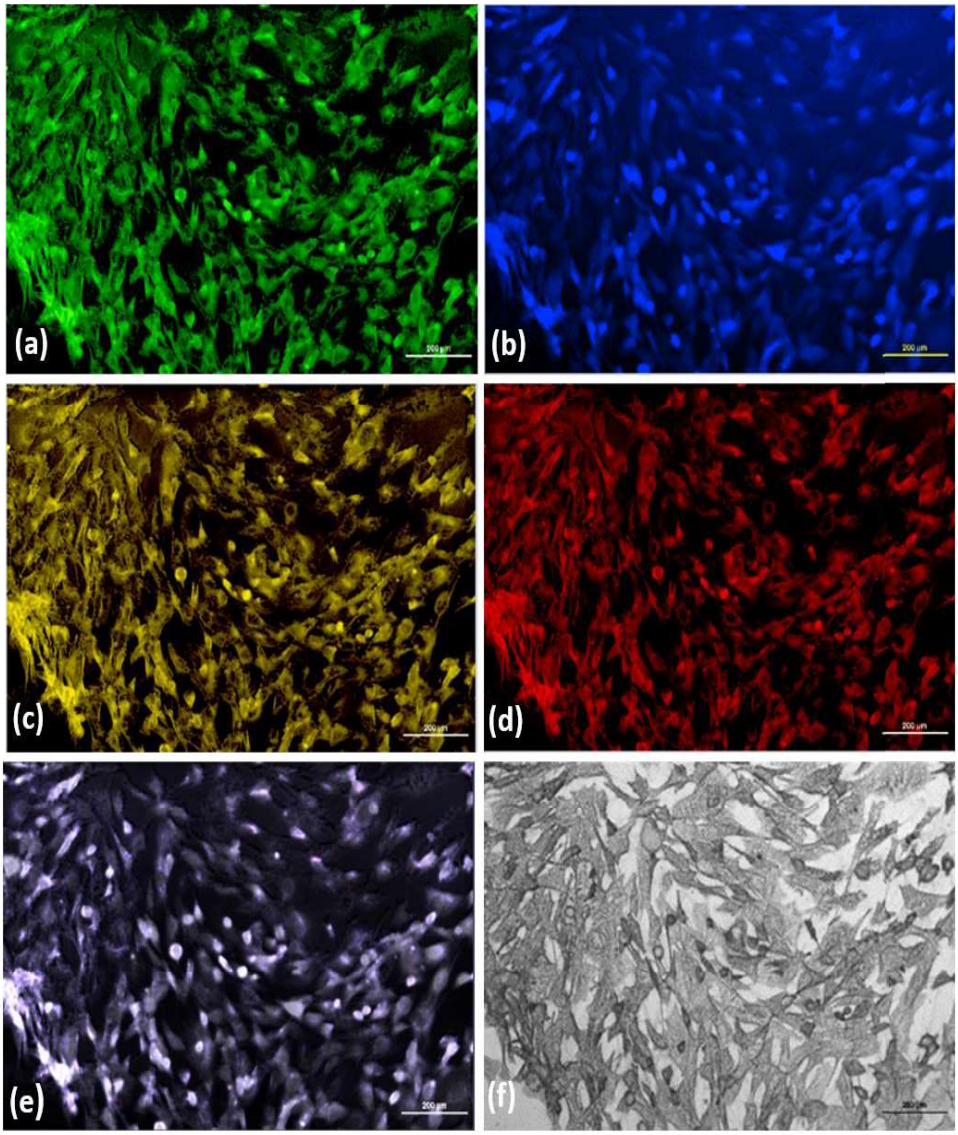

Figure 3.20 *In-vitro* multicolor fluorescent images of MG-63 cells incubated with FCPN (a) Ex./Em: 472/541 nm. (b) Ex./Em: 366 /477 nm. (c) Ex./Em: 516/595 nm. (d) Ex./Em: 472/ 636 nm. (e) merged. (f) bright field images.

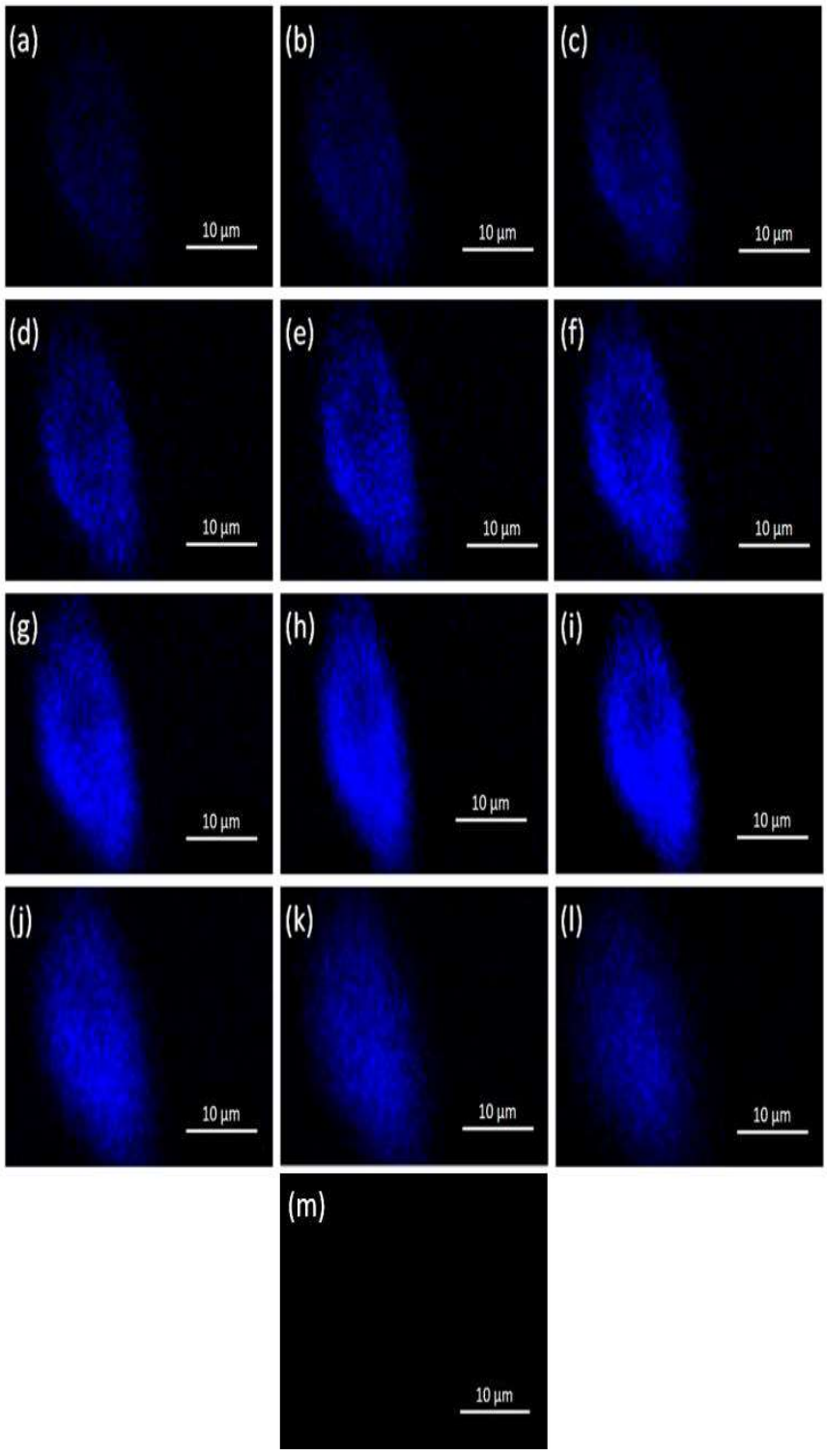
(a)
10 µm
(b)
10 µm
(c)
10 µm
(d)
10 µm
(e)
10 µm
(f)
10 µm
(g)
10 µm
(h)
10 µm
(i)
10 µm
(j)
10 µm
(k)
10 µm
(l)
10 µm
(m)
10 µm

Figure 3.21 Z stack confocal images of MG-63 cell incubated with FCPN (Ex.366 nm, Em. Blue). (a)= 0 µm. (b) = 2 µm. (c) = 4 µm. (d) = 6 µm. (e) =8 µm. (f) = 10 µm. (g) = 12 µm. (h) = 14 µm. (i) = 16 µm.(j) = 18 µm. (k) = 20 µm. (l) = 22 µm. (m) = control (culture media).

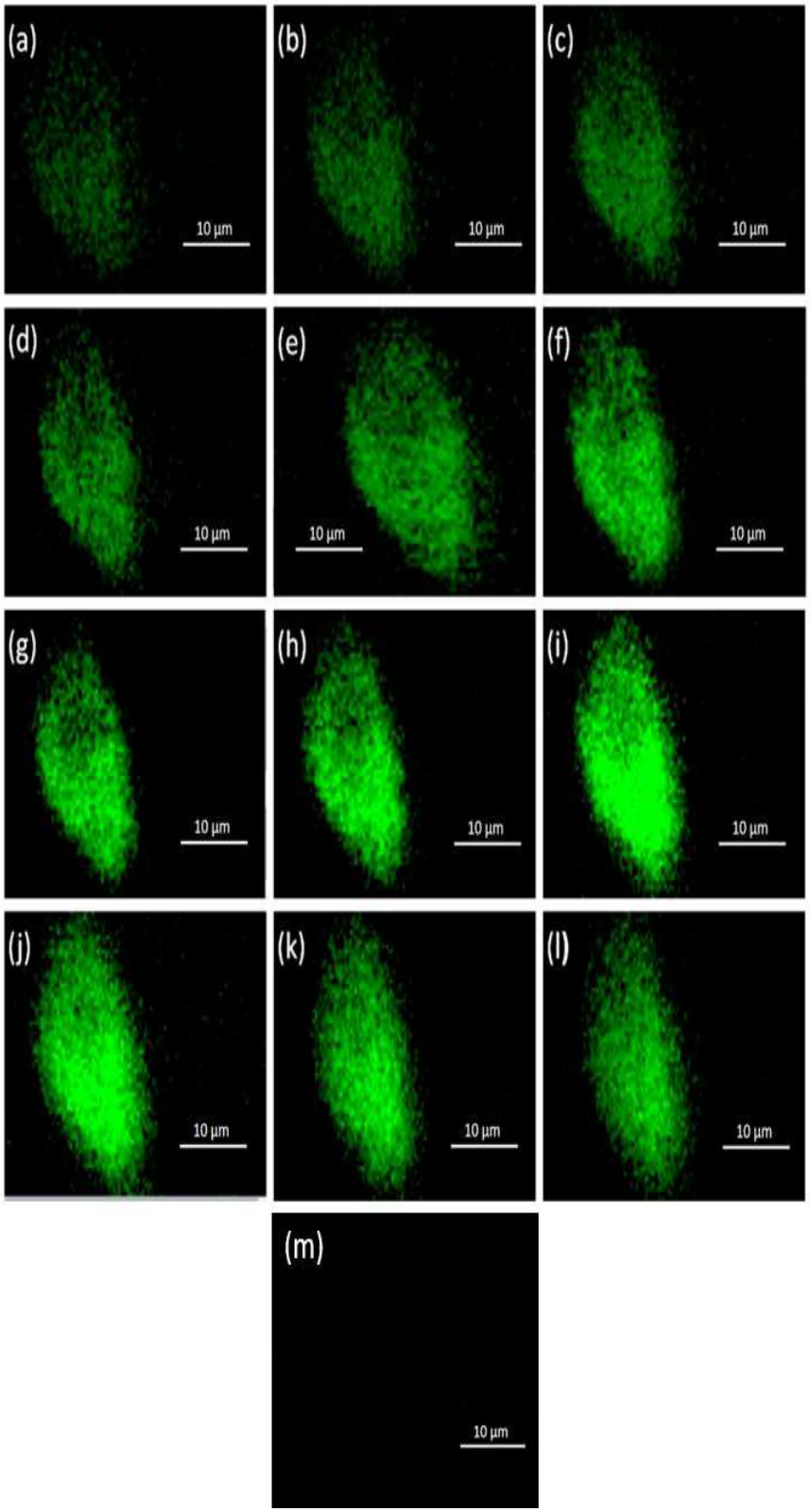

Figure 3.22 Z stack confocal images of MG-63 cell incubated with FCPN (Ex. 472 nm, Em. green). (a)= 0 µm. (b) = 2 µm. (c) = 4 µm. (d) = 6 µm. (e) =8 µm. (f) = 10 µm. (g) = 12 µm. (h) = 14 µm. (i) = 16 µm.(j) = 18 µm. (k) = 20 µm. (l) = 22 µm. (m) = control (culture media).

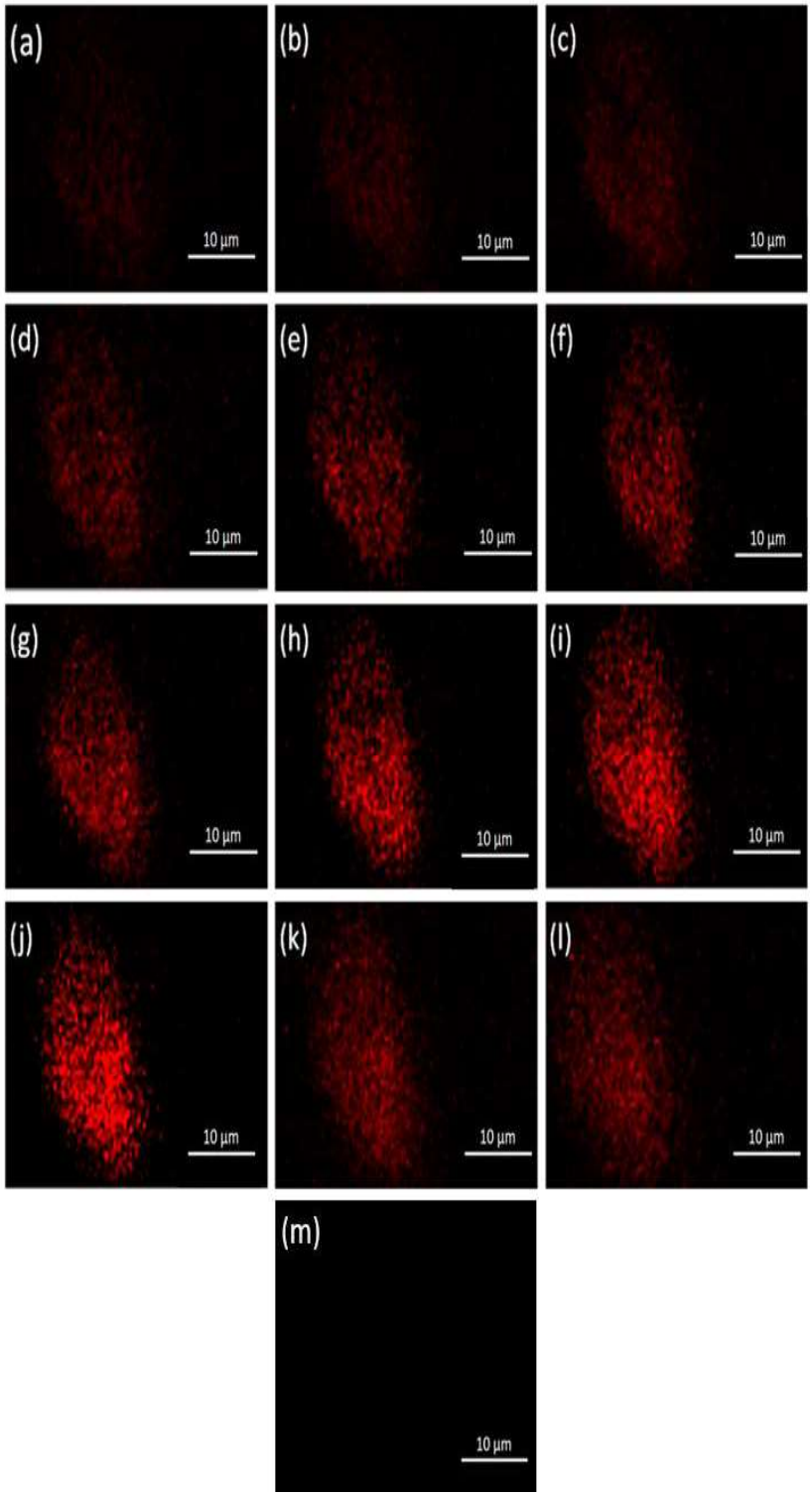

Figure 3.23 Z stack confocal images of MG-63 cell incubated with FCPN (Ex.472 nm, Em. Red) (a)= 0 µm. (b) = 2 µm. (c) = 4 µm. (d) = 6 µm. (e) =8 µm. (f) = 10 µm. (g) = 12 µm. (h) = 14 µm. (i) = 16 µm.(j) = 18 µm. (k) = 20 µm. (l) = 22 µm. (m) = control (culture media).

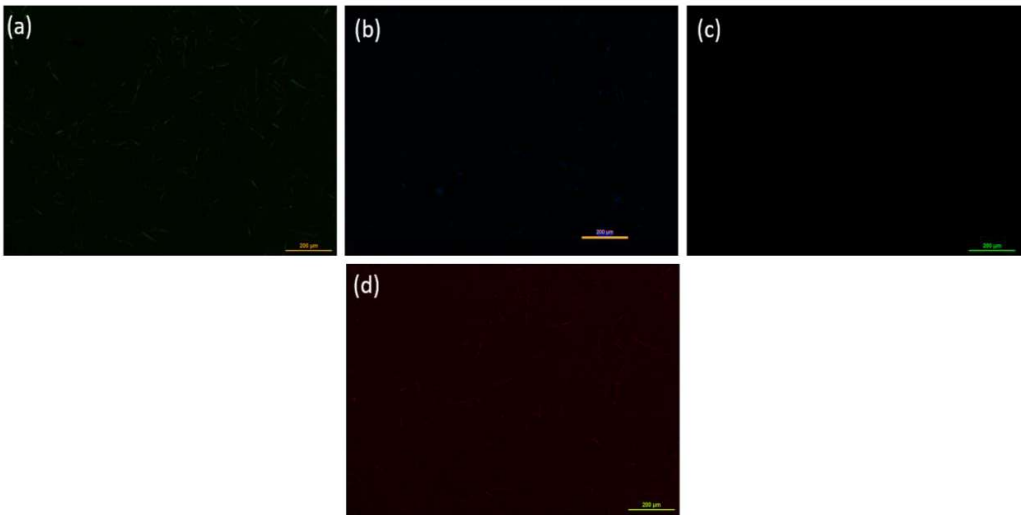

Figure 3.24 Fluorescent microscopy images of MG-63 cells incubated with culture media (control) (a) (Ex. 472 nm), (b) (Ex. 366 nm), (c) (Ex. 516 nm) (d) (Ex. 472 nm).The control images appear to be dark, due to lack of emission from the samples.

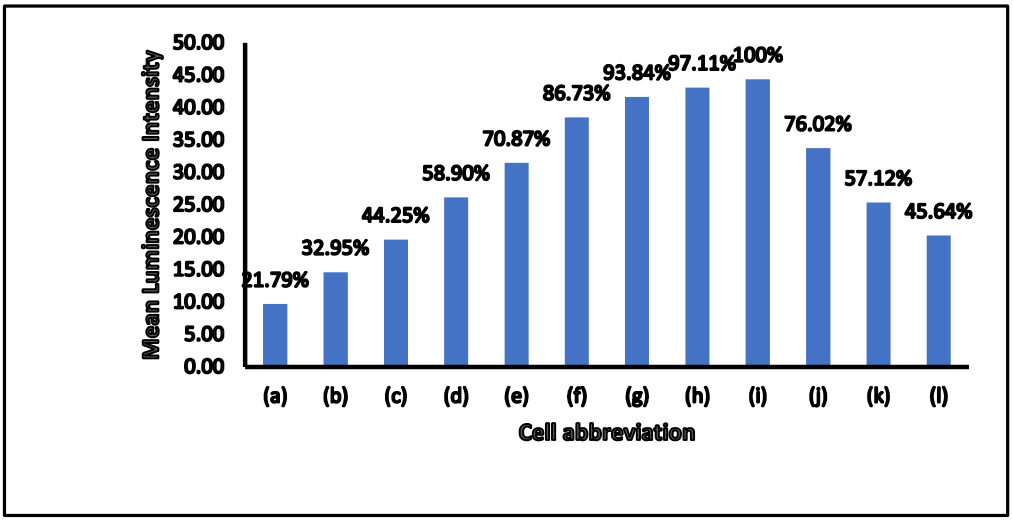
Mean Luminescence Intensity
50.00
45.00
40.00
35.00
30.00
25.00
20.00
15.00
10.00
5.00
0.00
21.79%
32.95%
44.25%
58.90%
70.87%
86.73%
93.84%
97.11%
100%
76.02%
57.12%
45.64%
(a) (b) (c) (d) (e) (f) (g) (h) (i) (j) (k) (l)
Cell abbreviation

(1)

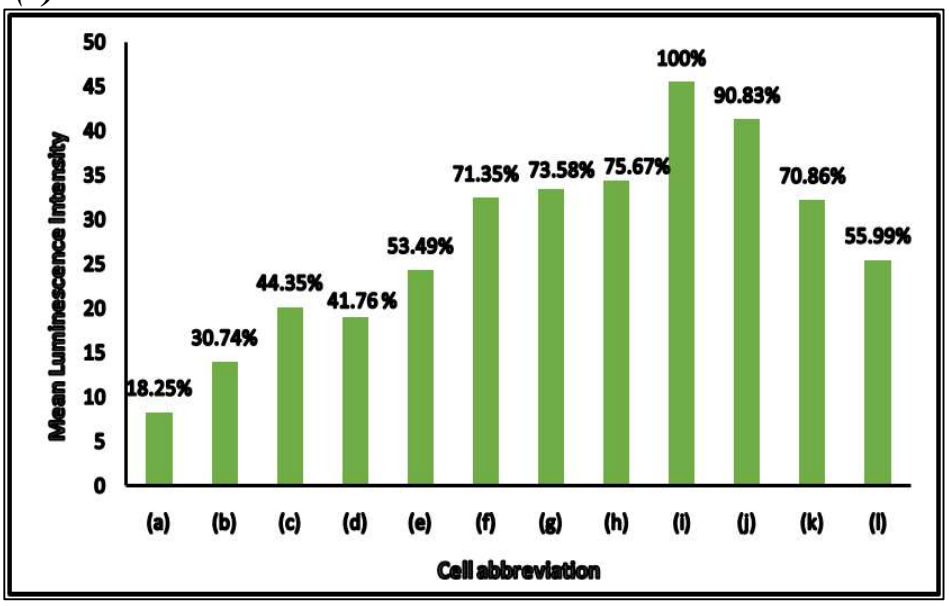
Mean Luminescence Intensity
50
45
40
35
30
25
20
15
10
5
0
18.25%
30.74%
44.35%
41.76 %
53.49%
71.35%
73.58%
75.67%
100%
90.83%
70.86%
55.99%
(a) (b) (c) (d) (e) (f) (g) (h) (i) (j) (k) (l)
Cell abbreviation

(2)

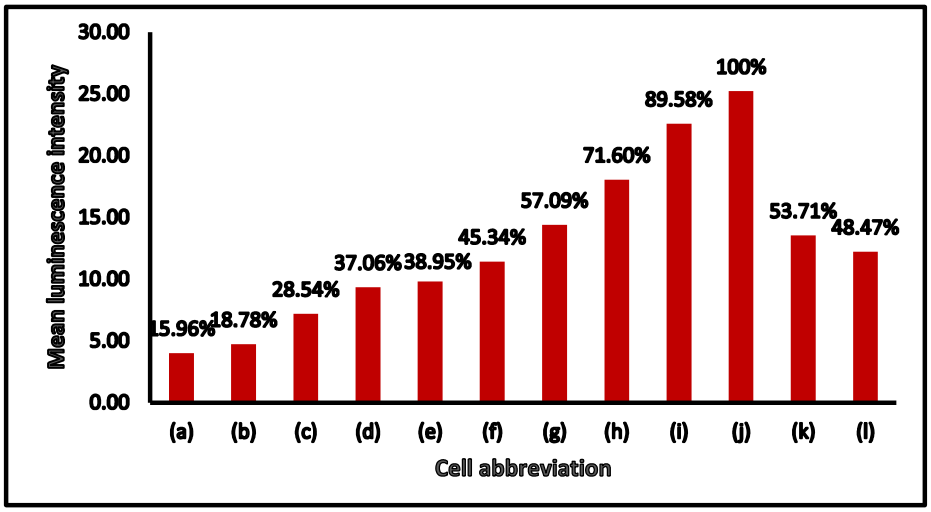

(3)

Figure 3.25 Mean Luminescence Intensity in MG-63 cells (1) FCPN [Ex. 366 nm, Em. Blue (477 nm)] (2) FCPN [Ex. 472 nm, Em. Green (541 nm)] (3) FCPN [Ex. 472 nm, Em. Red (636 nm)]: (a) = 0 µm, (b) = 2 µm, (c) = 4µm, (d) = 6 µm, (e) = 8 µm, (f) = 10 µm, (g) = 12 µm, (h) = 14 µm, (i) = 16 µm, (j) = 18 µm, (k) = 20 µm, (l) = 22 µm.

Conclusion

A facile method for the synthesis of a novel multi-color fluorescent BSA capped $CaCO_3$ prenucleation clusters using a green route is presented. Comprehensive spectrometric as well as microscopic means like TEM, HR-XRD, XPS, Fluorometer, Fluorescence microscope (Confocal as well) Fluorescence lifetme spectrometer etc. were used to detect the optical and compositional analysis of BSA capped $CaCO_3$ prenucleation nanoclusters.The resulting BSA capped $CaCO_3$ prenucleation nanoclusters were emerged as a promising tool for bio-imaging due to its excellent biocompatibility, high photostablity, pH stability and physiological stability. Such class of nanomaterial may facilitate instigation towards the development of novel and ingenious optical nanomaterials.

Table 2: Comparison table for biocompatibility, spectroscopic, physical, chemical and other properties for FCPN, Alexa Fluor organic dye, gold fluorescent cluster and magnesium fluorescent cluster.

Biocompatibility and Spectroscopic properties		FCPN	Alexa Fluor	Gold clusters	MgNCs
	Biocompatibility	-100% biocompatible -The decomposition products of $CaCO_3$ are water soluble, non toxic and can be easily excluded from the body.[396, 397]	-clinical usage is still confined because of its possible toxicity[398]	-(~85-90%) biocompatible[399] -After injecting BSA protected fluorescent gold nanocluster to the mice, vital organs such as liver and kidney got infected and damaged after 28 days[400]	-(~95%). biocompatible[401]
	Photo-stability	-YES, photostable (83 minutes) for all emissions. (~55 fold more photostable than Alexa Fluor)	-Alexa Fluor is Less Photostable (90 seconds only)[402]	-photo-stability drops to zero for blue emission (Au_7) and drops to approx. 15% for green emission (Au_{13}) as well as red emission (Au_{25}) after light exposure for 10,000 seconds[403]	-Photo bleaching data is not reported[401]
	Muticolor	-Yes (based on single fluorescent compound)	- Separate synthesis required for different color emissions for Alexa flour organic dyes	-Separate synthesis required for different emissions[403]	-Dual emission (blue and green)[401]
	Lifetime	-τ_{avg} =6.23 ns (green emission), τ_{avg} =30.6 ns (red emission), greater than the cell auto-fluorescence lifetime	-Lifetime (3.4 ns) lies within the cell autofluoresence lifetime (2−5 ns)[404]	-Lifetime: τ_{avg} =0.5 ns[399] (green emission) τ_{avg} =>100 ns[405] (red emission	-Not reported[401]

	Quantum Yield	-Quantum Yield (~0.0175) in water (H_20) for green emission relative to Rhodamine 6G (~0.90±0.2)[406]	-High Quantum Yield (~0.66)[407]	-Quantum yield (~0.012) for green emission[399]	-Quantum yield (~0.17) for blue emission[401]
Physical Properties	Size	-Ultrafine (~1 nm)	-Ultrafine(~0.4 nm)[408]	-Ultrafine (~2.6 ± 0.7 nm)[399]	-large size (~8.5 nm)[401]than FCPN, Alexa Fluor and Gold cluster
	Preparation	-One pot facile synthesis	-multistep synthesis procedure required[409]	-One pot facile synthesis.[399]	-One pot facile synthesis[401]
Chemical properties	Physiological Stability	-Yes (4 months)	-	-Yes (3 months)[410]	-Yes (4 months)[401]
	pH Stability	-Yes (5.8-12)	-Yes (4-10)[408]	-Yes (5-12.5)[411]	-Yes[401]
Other		-Low cost of synthesis than gold cluster synthesis due to cheap precursor ($CaCl_2$) than gold precursor.	-Much expensive[412] than FCPN, gold and magnesium cluster.	-Little expensive than FCPN and magnesium cluster.	-Low cost of synthesis